BRNO UNIVERSITY OF TECHNOLOGY

Faculty of Electrical Engineering
and Communication

MASTER'S THESIS

Brno, 2024 Bc. Matej Borovička

BRNO UNIVERSITY OF TECHNOLOGY

VYSOKÉ UČENÍ TECHNICKÉ V BRNĚ

FACULTY OF ELECTRICAL ENGINEERING AND COMMUNICATION

FAKULTA ELEKTROTECHNIKY
A KOMUNIKAČNÍCH TECHNOLOGIÍ

DEPARTMENT OF RADIO ELECTRONICS

ÚSTAV RADIOELEKTRONIKY

THERMAL MANAGEMENT FOR MISSION CIMER

TERMÁLNÍ MANAŽMENT PRO MISI CIMER

MASTER'S THESIS
DIPLOMOVÁ PRÁCE

AUTHOR
AUTOR PRÁCE

Bc. Matej Borovička

SUPERVISOR
VEDOUCÍ PRÁCE

doc. Ing. Tomáš Götthans, Ph.D.

BRNO 2024

BRNO UNIVERSITY OF TECHNOLOGY
FACULTY OF ELECTRICAL ENGINEERING AND COMMUNICATION

Master's Thesis

Master's study program **Space Applications**

Department of Radio Electronics

Student: Bc. Matej Borovička ***ID:*** 208436

Year of study: 2 ***Academic year:*** 2023/24

TITLE OF THESIS:

Thermal management for mission CIMER

INSTRUCTION:

Study the issue of thermal numerical simulations in space applications. Create a geometric and thermal model of the satellite for the CIMER mission. Analyze thermal external factors affecting the satellite in low Earth orbit. Analyze the temperature distribution inside the orbiting satellite. Focus on the effect of satellite orientation, surface properties, and orbital parameters.

RECOMMENDED LITERATURE:

[1] FOSTER, Isaac. Small Satellite Thermal Modeling Guide. Online PDF. RG.2.2.35225.29288. 2022. Dostupné také z: https://apps.dtic.mil/sti/pdfs/AD1170386.pdf.

[2] MIAO, Jianyin; ZHONG, Qi; ZHAO, Qiwei a ZHAO, Xin. Spacecraft Thermal Control Technologies. Online. Space Science and Technologies. Singapore: Springer Singapore, 2021. ISBN 978-981-15-4983-0. Dostupné z: https://doi.org/10.1007/978-981-15-4984-7.

[3] Thermal analysis handbook. Online PDF. ECSS-E-HB-31-03A. 2016. Dostupné také z: https://ecss.nl/home/ecss-e-hb-31-03a-15november2016/.

Date of project specification: 16.2.2024 ***Deadline for submission:*** 20.5.2024

Supervisor: doc. Ing. Tomáš Götthans, Ph.D.
Consultant: Ing. Martin Mačák, Ph.D.

doc. Ing. Tomáš Götthans, Ph.D.
Chair of study program board

Abstract

This thesis deals with the thermal analysis of the CubeSat, the evaluation and subsequent implementation of the results in the satellite design itself is very important to ensure the proper functioning of all its components. The first part describes thermal analysis issues and proposals for space applications. The second part is devoted to the thermal design of the CIMER nanosatellite, whose mission is to cultivate cyanobacteria in low Earth orbit. Cyanobacteria have very specific requirements in terms of the temperature range in which they can survive. This analysis is therefore very important for the functioning of the entire mission. The thesis describes the creation of a thermal design in the software Systema Thermica, its subsequent analysis and evaluation. Finally, the model is adapted to the conditions required for the survival of cyanobacteria in space.

Keywords

Cubesat, Nanosatellite, Thermal analysis, Thermal model, Systema Thermica

Abstrakt

Táto práca sa zaoberá tepelnou analýzou CubeSatu, pričom vyhodnotenie a následná implementácia výsledkov do samotnej konštrukcie družice je veľmi dôležitá na zabezpečenie správneho fungovania všetkých jej komponentov. V prvej časti je opísaná problematika tepelnej analýzy a návrhy pre vesmírne aplikácie. Druhá časť je venovaná tepelnému návrhu nanosatelitu CIMER, ktorého úlohou je kultivácia cyanobaktérií na nízkej obežnej dráhe Zeme. Sinice majú veľmi špecifické požiadavky, pokiaľ ide o teplotný rozsah, v ktorom môžu prežiť. Táto analýza je preto veľmi dôležitá pre fungovanie celej misie. Práca opisuje vytvorenie tepelného návrhu v softvéri Systema Thermica, jeho následnú analýzu a vyhodnotenie. Nakoniec je model upravený na podmienky potrebné na prežitie siníc vo vesmíre.

Klíčová slova

Cubesat, Nanosatelit, Termálna analýza, Termálny model, Systema Thermica

Rozšířený abstrakt

Táto práca sa zameriava na tepelnú analýzu CubeSatu, pričom zdôrazňuje dôležitosť správneho tepelného návrhu pre zabezpečenie optimálneho fungovania jeho komponentov. V teoretickej časti sú predstavené základné princípy prenosu tepla a výzvy, ktorým CubeSaty čelia vo vesmírnom prostredí. Táto časť tiež popisuje nástroje a metódy používané na riešenie tepelných problémov, vrátane softvéru Systema Thermica.

Praktická časť práce sa sústreďuje na nanosatelit CIMER, ktorého cieľom je kultivácia cyanobaktérií na nízkej obežnej dráhe Zeme. Cyanobaktérie majú veľmi špecifické požiadavky na teplotný rozsah, v ktorom môžu prežiť, čo robí tepelný dizajn tejto misie kľúčovým pre jej úspech. Proces tvorby tepelného modelu CIMER v softvéri Systema Thermica je podrobne popísaný, vrátane analýzy a vyhodnotenia výsledkov. Na základe získaných dát sú vykonané potrebné úpravy modelu na zabezpečenie optimálnych podmienok pre prežitie cyanobaktérií vo vesmíre.

Praktická časť zahrnuje modelovanie všetkých subsystémov satelitu a ich tepelnú analýzu. Výsledky tejto analýzy sú následne vyhodnotené a interpretované s cieľom overiť, či návrh spĺňa požadované teplotné podmienky pre celú misiu. Záverečná časť práce prináša podrobný popis dosiahnutých výsledkov a ich význam pre ďalší vývoj satelitných technológií.

Bibliographic citation

BOROVIČKA, Matej. *Termální manažment pro misi CIMER* . Brno, 2024. Dostupné také z: https://www.vut.cz/studenti/zav-prace/detail/160097. Diplomová práce. Vysoké učení technické v Brně, Fakulta elektrotechniky a komunikačních technologií, Ústav radioelektroniky. Vedoucí práce Tomáš Götthans.

Author's Declaration

Author:	Bc. Matej Borovička
Author's ID:	208436
Paper type:	Master's Thesis
Academic year:	2023/24
Topic:	Thermal management for mission CIMER

I declare that I have written this paper independently, under the guidance of the advisor and using exclusively the technical references and other sources of information cited in the project and listed in the comprehensive bibliography at the end of the project.

As the author, I furthermore declare that, with respect to the creation of this paper, I have not infringed any copyright or violated anyone's personal and/or ownership rights. In this context, I am fully aware of the consequences of breaking Regulation S 11 of the Copyright Act No. 121/2000 Coll. of the Czech Republic, as amended, and of any breach of rights related to intellectual property or introduced within amendments to relevant Acts such as the Intellectual Property Act or the Criminal Code, Act No. 40/2009 Coll., Section 2, Head VI, Part 4.

.

Brno, May 19, 2024 ----------

author's signature

Acknowledgement

I would like to thank my thesis supervisor Doc. Ing. Tomáš Götthans Ph.D. and especially consultant Ing. Martin Mačák Ph.D. for their professional guidance, valuable advice, and comments during the preparation of this thesis. I also thank Airbus Defense and Space for granting me a license for the Systema Thermica software, in which this thesis was prepared. In addition, I acknowledge the use of artificial intelligence in the firmatting of the text in this thesis.

Brno, May 19, 2024 ----------

Author's signature

Contents

FIGURES

TABLES

INTRODUCTION

Since ancient times, the exploration of the universe has been a source of enrichment for mankind's knowledge of how the world works. However, the most significant advance came with the launch of the first satellite into space. Since then, our understanding of the universe has grown exponentially, taking us to a new technological frontier. The advent of satellites has enabled the precise location of mobile devices, the spread of the internet and the ability to see the current weather at any time through satellite images. Satellites are used to analyse a wide range of phenomena on the planet, including the thickness of the ozone layer, soil fertility and military applications. The development of satellite technology has made it impossible to imagine life without it. It is therefore clear that the progress of our society and economy depends on the continued development of satellites.

However, the environment in which satellites are located is inhospitable. Consequently, they must be highly resilient and prepared for all the potential challenges posed by this environment. One such factor is temperature. It is important for satellites to withstand extreme temperature fluctuations, as their equipment is particularly vulnerable, making it essential to ensure the satellite's design is robust enough to protect its equipment and maintain operational status. This is addressed by thermal analyses, which have the task of predicting the thermal behaviour of the individual components of the satellite from the properties of the environment and the satellite itself. This then allows the satellite to be adjusted so that it is prepared for any eventuality.

The objective of this study is to develop a thermal model for the CIMER mission, which is tasked with cultivating cyanobacteria in orbit. The bacteria in question produce oxygen during their cultivation, which is an essential element of life for us. This experiment may therefore contribute to the future exploration of space by man himself, as it would facilitate the production of oxygen even on long spacecraft flights to other planets. These bacteria are highly resilient to a range of external factors, yet they are particularly susceptible to fluctuations in temperature during cultivation. Consequently, thermal design represents a pivotal component in ensuring the successful execution of this mission.

The specific objectives of this study are to conduct a thermal analysis of the entire CubeSat CIMER, including its payload in software Systema Thermica. The basic architecture of the payload must be designed in such a way that it meets the specified temperature requirements. This will enable the verification of whether it is possible to carry out the mission in accordance with the current plan.

This thesis begins with an introduction to the topic of CubeSats, followed by an explanation of the basic physical background of heat transfer. Subsequently, it describes the conditions that CubeSats face in the space environment. The tools used to address issues in thermal management are then discussed. An important section is the explanation of the calculations for thermal simulations and the operation of the relevant software. In

the practical part, all subsystems of the satellite are described and then modelled in thermal software. This thermal model is evaluated, and necessary adjustments are implemented to meet the model's requirements. The thesis concludes with a detailed description of all analysis results and their evaluation.

1. CUBESATS

In the 1990s, the size of satellites in orbit began to increase significantly. The aim was to reduce the cost per kilo of material carried into space by installing as many synergistic measuring instruments as possible on large satellites. However, there were various problems related to micro-vibrations, electromagnetic compatibility of measuring instruments, etc. So small satellites took their turn. Breakthroughs in technology have made it possible to reduce the size of the basic components for satellite functionality. In 1999, Professor Jordi Puing-Suari and Bob Twiggs at California Polytechnic State University established the specifications for the first 1U or 10x10x10 cm CubeSat. These dimensions have become standardized and each CubeSat always consists of several units, such as: 1.5U, 2U, 3U, 6U and 12U. The assembly of 1U CubeSats is shown in the next Figure 1.1. [1] [2]

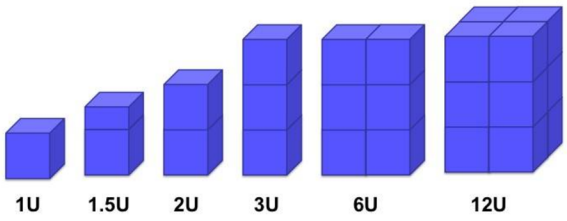

Fig. 1.1: CubeSat sizes [2]

These standardised dimensions allow for easy and safe placement in so-called deployers. The first and one of the most widely used is the P-POD, which was developed at Cal Poly. These devices serve as the interface between the CubeSat and the launch vehicle. Their function is to protect the satellite during the launch of the rocket and then launch them into the correct orbit at the optimal moment, employing a spring mechanism.

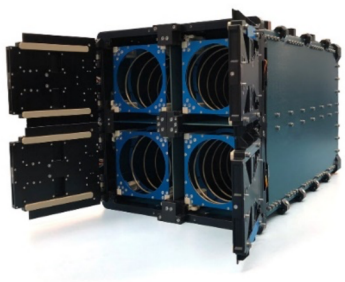

Fig. 1.2: CubeSat deployer [3]

Thanks to these capabilities, the possibility of sending satellites into space was significantly enhanced, and the number of launched nanosatellites began to grow annually. [1] [2][17]

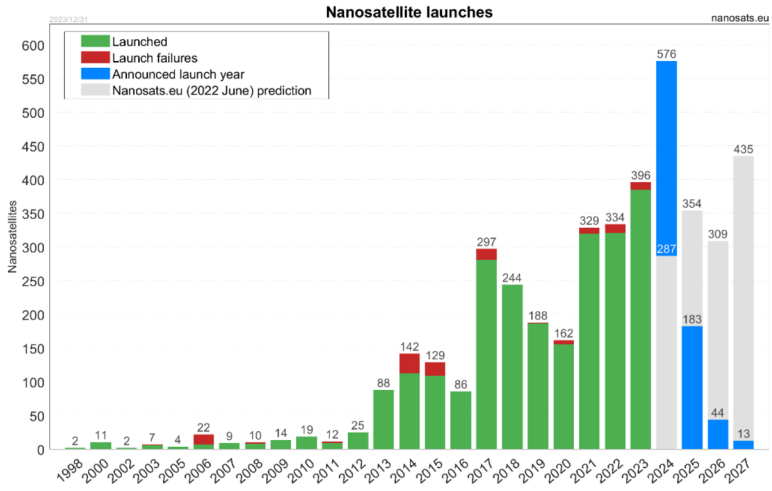

Fig. 1.3: Nanosatellite launches [4]

Figure 1.2 shows a significant rise in nanosatellite launches in recent years. This is primarily due to the improved computational performance of smaller devices. As a result, nanosatellites can sometimes provide better observational results than standard ones. Affordability is another reason for the increase in launches, making it possible to launch student satellites for research and scientific purposes. [1]

In the past, nanosatellites did not need complex thermal management. The first CubeSats were mostly just test facilities for new components. They had low power consumption and a short lifetime. With 1U CubeSats, the electronics can heat themselves enough to stay within operating temperatures. Nowadays, CubeSats are much more complex and thus much more attention needs to be paid to thermal management. [5]

2. HEAT TRANSFER

To understand the thermal behaviour of a satellite, it is important to explain the basic principles of heat transfer. Heat is transferred through radiation, conduction, and convection. Radiation and convection significantly affect the temperature of the uniform parts of the satellite. Convection involves the transfer of heat through the flow of molecules in fluids, which is not applicable in space due to the vacuum.

2.1.1 Conduction

Conduction is the transfer of heat through collisions between atoms and molecules in a substance. It is most significant in solids and least in gases. The rate of heat transfer depends on the material's conductivity k and the temperature gradient dT/dx between cold and warm parts. This is described by the following equation, which is only valid for homogeneous materials: [7]

$$q_k = -kA\frac{dT}{dx}, \tag{2.1}$$

A is the area through which heat is transferred. The minus sign means that heat always flows from the warmer part to the cooler part. This is based on the second law of thermodynamics. Conductivity k is a material property and is the amount of heat that can pass through a unit area of material per unit time at a unity temperature gradient. [6][7]

2.1.2 Radiation

Any object with a temperature above absolute zero emits electromagnetic radiation. This radiation can be converted into heat when it is absorbed by another object. The amount of energy emitted by body can be calculated using Planck's radiation law: [6]

$$E = hf, \tag{2.2}$$

where h is Planck's constant, and f is the frequency of the electromagnetic radiation. This law states that radiation can only be emitted or absorbed in quanta. Based on this principle, a relation for the spectral radiance of a perfectly black body was derived:[6]

$$E_0(\lambda, T) = \frac{2hc^2\lambda^{-5}}{e^{\frac{hc}{\lambda T k}}-1}, \tag{2.3}$$

where c is the speed of light in a vacuum, k is Boltzmann's constant λ is the wavelength of the radiation and T is the temperature of the body in Kelvins. The meaning

of this relationship is best explained in Figure 2.1, which shows that the amount of spectral energy radiated increases with temperature of the radiating body and at the same time the wavelength of radiation at which the body radiates the most decreases.

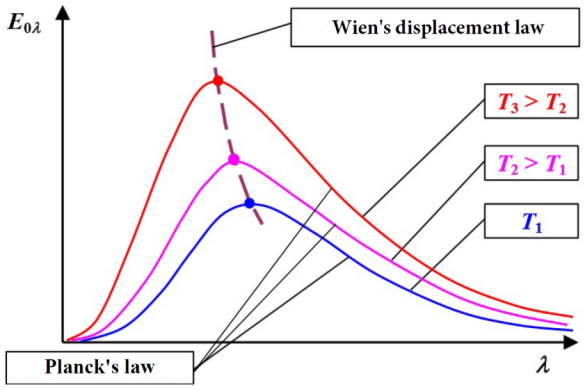

Fig. 2.1: Plot of spectral density as a function of temperature and wavelength [6]

Wien's displacement law was derived from Planck's radiation law to determine the maxima of the wavelengths at which a body radiates, giving the inverse proportionality between the temperature of the body and the wavelength of the radiation:[6]

$$\lambda_{max} = \frac{b}{T}, \tag{2.4}$$

where b is Wien's constant.

2.1.3 View Factor

In order to approximate the behaviour of radiation between several bodies, it is necessary to consider not only the overall physics of radiation, but also the geometry of the system in which the bodies are located. This is described by the view factor, which can be defined as the fraction of diffusely distributed radiation that leaves surface A1 and reaches surface A2. The view factor can be calculated using the following equation: [7]

$$F_{12} = \frac{1}{\pi A_1} \iint \frac{\cos\theta_1 \cos\theta_2}{\pi r^2} \, dA_1 dA_2 \,, \tag{2.5}$$

The elements on surfaces 1 and 2 are represented by dA_2 and dA_2, respectively. The distance between element dA_1 and dA_2 is defined by r, θ_1 and θ_2 are the angles between the line connecting the elements and the normal of surface 1 and 2, respectively. and A_1 and A_2 are the areas of surfaces 1 and 2, respectively.

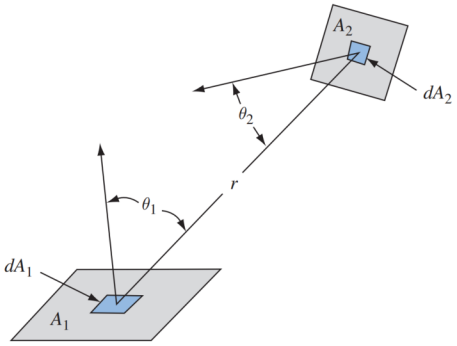

Fig. 2.2: Schematic picture for view factor derivation [7]

The view factor F_{12} has three important properties: unity, reciprocity, and superposition. Calculating the view factor serves as the foundation for other radiation analyses, such as radiative exchange factor and orbital heating. [6] [7]

2.1.4 Black and Grey Body Radiation

The amount of energy leaving the surface as radiant heat, called the heat flow rate q_r, is defined by the Stefan-Boltzmann law.[6]

$$q_r = \sigma A T^4 \tag{2.6}$$

The resulting value is in watts and is proportional to the fourth power of the body temperature T, given in Kelvin. The Stefan-Boltzmann constant σ has a value of 5.67×10^{-8} W.m^{-2}K^{-4}. A represents the surface area of the body. This law describes the radiation from a perfect black body. In other words, a body that perfectly absorbs all incoming electromagnetic radiation and then continuously radiates the entire spectrum into the environment.

However, there are no perfectly black bodies. To approximate the properties of real bodies, the grey body model is used. A grey body emits and absorbs less radiation than a perfectly black body. The ratio of these radiations is expressed by the emissivity and absorptivity, which range from 0 to 1, where 1 represents a black body. Figure 2.3 shows a comparison of the radiated energy at each wavelength for a blackbody, a graybody, and a real surface.

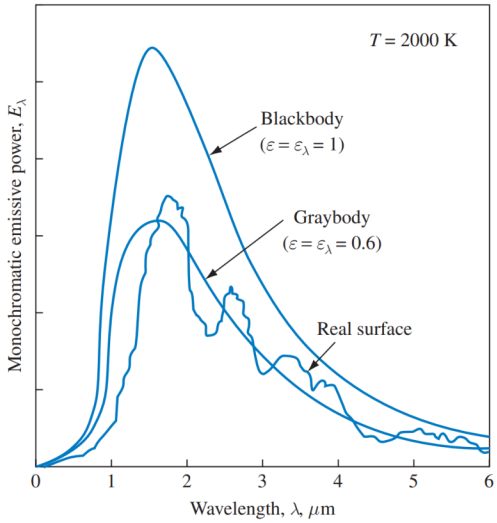

Fig. 2.3: Comparison of monochromatic emissive power for a black, a grey and a real body [7]

Since the Sun can be considered as a black body, this principle facilitates the computation of its radiant power. The surface temperature of the Sun is 5780K and its radius is 695.7×10^6 m. [8]

$$P = 4\pi r^2 \sigma T^4 \tag{2.7}$$

The sun's radiant power, also known as total power of Sun P, is equal to: 3.85×10^{26} W.

Based on the above laws, it can be concluded that all real bodies are emitters of energy. Therefore, when calculating a body's energy loss, it is crucial to consider the surrounding environment, which also emits energy. The following equation can be used to determine the net heat flow of a grey body in a black enclosure, as shown in the Figure 2.4: [14]

$$q_{net} = A_1 \varepsilon_1 \sigma (T_1^4 - T_2^4) \tag{2.8}$$

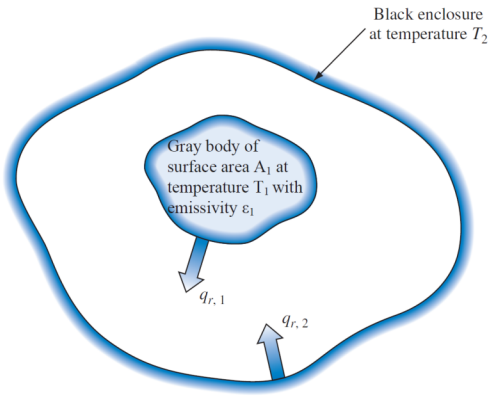

Fig. 2.4: Schematic diagram of radiation between grey body and black enclosure [7]

The emissivity of the grey body is represented by ε_1. This arrangement can also be used to describe the cooling of spacecraft in free space, where the space background can be considered as a perfectly black body with a temperature of 2.7 K. This arrangement can only be used in certain cases. In most cases, surrounding bodies such as the Earth or the Sun must also be considered. These bodies almost always radiate energy to the satellite at some angle and illuminate only some part of it. In this case, a more complex relationship is needed which takes into account the mutual irradiance of two grey faces, described by the view factor F_{12}. [6] [7] [9]

$$q_{12} = \frac{\sigma(T_1^4 - T_2^4)}{\frac{1-\varepsilon_1}{\varepsilon_1 A_1} + \frac{1}{A_1 F_{12}} + \frac{1-\varepsilon_2}{\varepsilon_2 A_2}} \tag{2.9}$$

3. SPACE ENVIRONMENT

Space is a highly inhospitable environment. The mean temperature of space is -270.45 °C. However, the satellite's position undergoes rapid changes, particularly with regard to its orbit around the Earth. The most commonly utilised orbits are Low Earth Orbit (LEO), Medium Earth Orbit (MEO) and Geostationary Orbit (GEO). Each of these orbits has a specific temperature profile that depends on the distance from the Earth. This will affect the orbital period, the time spent in the shadow of the Earth, and so on. Figure 3.1 illustrates that the temperature is influenced by a number of factors, including solar radiation, albedo, infrared radiation from the Earth and radiation from the satellite into space. Other potential sources of heat include friction with free particles in the upper layers of the atmosphere or interaction with charged particles near the Van Allen belts. Nevertheless, these factors are relatively minor, particularly for smaller CubeSats, and may be disregarded. [11] [12] [13][14]

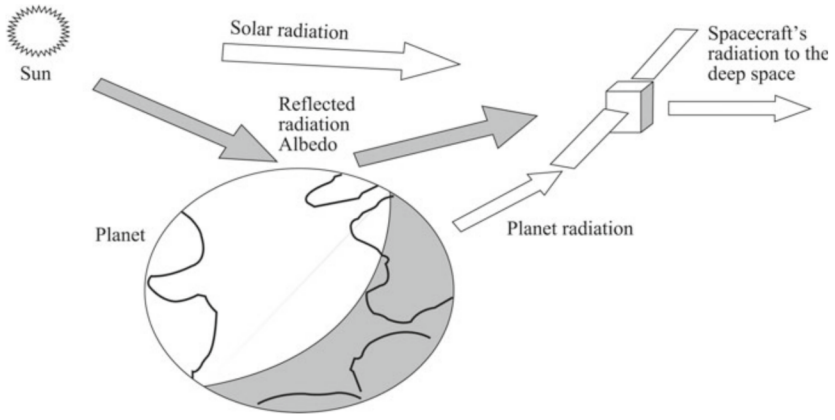

Fig. 3.1: Typical spacecraft thermal environment [11]

3.1 Thermal Environment in Low Earth Orbit

This work focuses on the low Earth orbit environment where our CubeSat CIMER will be deployed. Temperature changes in this region are extreme, ranging from -65°C to +125°C. [10]

3.1.1 Solar Radiation

In Low Earth Orbit (LEO), the Sun is the primary source of heat. The magnitude of incoming radiation varies around ±3.5%. At 1AU, the mean distance between the Earth and the Sun, the solar radiation intensity incident perpendicularly on the surface of the satellite is 1.367 $W.m^{-2}$, also known as the solar constant. The solar radiation intensity is

at its smallest, 1.322 W.m^{-2}, when the Earth is in summer in aphelion and at its highest, 1.414 W.m^{-2}, in winter in perihelion. The dependence of solar radiation intensity on distance from the Sun is described by the following formula: [8]

$$q_{solar} = \frac{P}{4\pi d^2} \tag{3.1}$$

where q_{solar} represents solar radiation intensity. The variable d is distance of the Earth from the Sun. [8] [11] [15]

Solar radiation can be roughly divided into 47% infrared, 46% visible and 7% ultraviolet radiation.

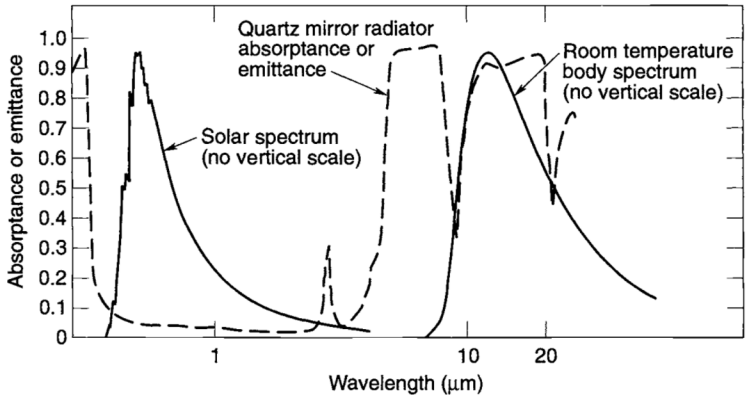

Fig. 3.2: Curve of radiation intensity of solar spectrum [8]

The graph shows that the Sun emits mainly at wavelengths between 0.76 and 2 μm in the IR part, while a body at room temperature radiates at wavelengths between 8 and 15 μm. [8] [11] [16]

3.1.2 Earth Albedo Radiation

Albedo radiation describes the reflected solar radian off the Earth. Sunlight is reflected in two ways: by scattering on molecules of gases and dust in the atmosphere, and by reflection from the Earth's surface. The ratio between these reflections is called the albedo ratio, which is influenced by various factors, including the angle at which the Sun's rays strike the Earth's atmosphere and surface. Perpendicular rays pass through the atmosphere more easily and are absorbed. As the angle increases, the atmosphere becomes more reflective. This causes the albedo to vary significantly over time and depends on latitude, longitude, weather, and the reflectivity of the Earth's surface. Table 3.1 shows examples of the reflectance values of different Earth surfaces.

Table 3.1: Reflectance values of various Earth surfaces [17]

Surface type	Reflectance
Freshly fallen snow	0.9
Melting Snow	0.4
Dirty Snow	0.2
Trees	0.09 - 0.18 (Depending on moisture and snow coverage)
Clouds	0-0.8
Water	Depends on - water texture (wavy vs. calm) - incident angle of radiation - polarization of light - frequency of radiation

The reflectivity values can vary during an orbit, making it difficult to predict exact values for the satellite mission.

The formula for calculating Earth albedo radiation intensity incident on the surface of a spacecraft is: [8]

$$q_{albedo} = A_f F S \tag{3.2}$$

where A_f represents the albedo factor which depends on Earth's surface reflectance, F is the view factor between the spacecraft surface and the Earth, and S is the solar radiation intensity incident on the Earth's surface. [8][11]

3.1.3 Earth's Infrared Radiation

A third significant source of heat in orbit is Earth's infrared radiation. Similar to albedo, the IR value varies with various factors: the distance of the earth from the sun, the earth's rotation, the geographical position and also with the weather. The changing temperature of Earth's surface is mostly caused by the alternation of day and night. Of course, different surfaces have different thermal inertia. The ocean changes its radiation less than the desert during the day, and at the poles the temperature hardly changes at all. Radiation itself is most affected by weather. Clouds block radiation from the surface of the earth very well and their tops are cool. All these factors cause the infrared radiation emitted by the earth for an orbiting satellite to vary. For simplicity it can be assumed that the Earth as a whole emits thermal radiation with a spectrum like a perfectly black body with an average temperature of 255K. Similarly to the calculation of total power of Sun it can be calculated the Earth radiation intensity at its surface what is equal to 1.22×10^{16} W.

$$P_{Earth} = 4\pi R_{Earth}^2 \sigma T_{Earth}^4 \tag{3.3}$$

Then it easy to determine radiation intensity for any orbit:

$$q_{EarthIR} = \frac{P_{Earth}}{4\pi(R_{earth}+h)^2} \quad (3.4)$$

For an orbit with a heigh above the surface of 500 km, the Earth's radiation intensity is equal to 206,15 W/m^2. [8][11][18]

4. THERMAL CONTROL SYSTEMS

Thermal control systems (TCS) is essential for spacecraft to maintain operational temperatures in the harsh environment of space. For CubeSats, effective thermal management is critical due to their small size and limited capacity for thermal regulation hardware. As previously described, a satellite in orbit is exposed to several sources of heat and at the same time emits it into the cold space. Each component of the satellite has a range of temperatures within which it is able to fully function. The objective of the thermal system is to maintain the temperature of all subsystems within their optimal operating range. This can only be achieved if, during the orbit, the heat flow through the satellite reaches equilibrium, as described by the following relationship: [19]

$$q_{solar} + q_{albedo} + q_{EarthIR} + Q_{gen} = Q_{stored} + Q_{out} \quad (4.1)$$

Q_{gen} is heat generated by spacecraft electrical components due to power dissipation, $Q_{out}$is heat emitted to surrounding cold space and Q_{stored} is heat stored by parts of spacecraft. Two principal methods exist for attaining this equilibrium: passive and active thermal control. These technologies have been developed for larger spacecraft, and over time, they have been scaled down and adapted for use in nanosatellites. [19]

4.1 Passive Thermal Control Systems

Passive thermal control systems are of great importance in maintaining the temperature of spacecraft within acceptable limits, without the need for power or active feedback mechanisms. These systems rely on the inherent physical properties of materials and structural designs to regulate heat transfer and thermal radiation. They are highlighted for their simplicity, reliability, universality and longevity. Various techniques, such as thermal coatings, heat conduction materials, thermal insulation, heat pipes and phase change materials, are commonly used in passive thermal control systems. [11][19]

4.1.1 Thermal Coatings

Coatings represent the fundamental means of influencing the effect of radiation on the temperature of the satellite. The thermo-optical characteristics of surfaces can be altered, enabling significant changes to be made to their absorptivity and emissivity. This allows for a substantial modification of the heat flow received by the satellite from the sun, as well as the heat exchange between different parts of the spacecraft and the loss of heat by

radiation to the surroundings.

Thermal coatings make use of the spectral properties of emitted light. Since the sun emits most of its thermal radiation at shorter wavelengths than objects at room temperature, it is advisable to choose a surface that reflects shorter wavelengths and emits longer ones well.

When selecting a coating, the length of the mission and the environment in which the satellite will operate must be considered. Coatings degrade over time and lose their original properties due to environmental influences. Specific to LEO is the erosion caused by oxygen atoms in the upper part of the atmosphere. Degradation is also caused by UV radiation and incident charged particles. For example, Figure 4.1 shows an experiment with white paint exposed on the ISS. It can be seen how the absorption of the paint increases over time due to the conditions mentioned above.

In order for the coatings to meet all the necessary requirements and at the same time be resistant to the environment, they are combined in various striped and checkered patterns.[11][17][21][26]

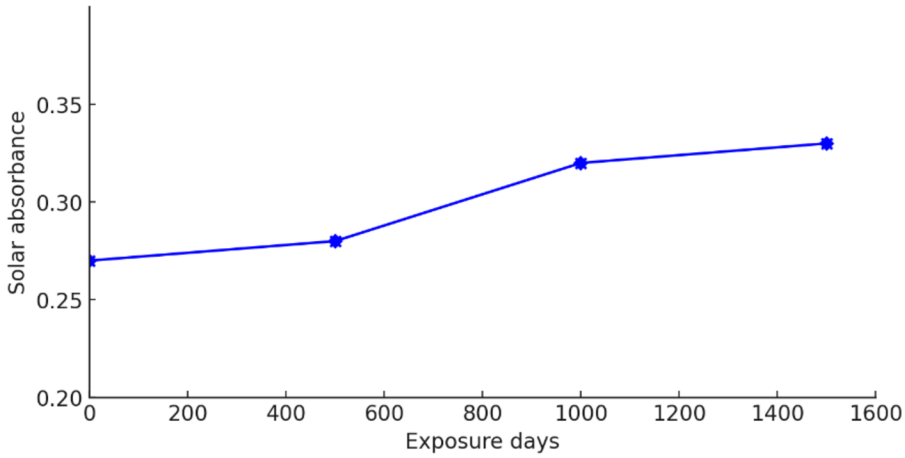

Fig. 4.1: Solar absorptance changes of white paint in ISS Russian service module space environment exposure device experiment [21]

4.1.2 Insulation

The most common type of insulation is Multi-Layer Insulation (MLI), which is primarily used as radiation insulation to limit the heat exchange between the spacecraft and the environment. It consists of several layers of thin reflective materials with low IR emissivity, mostly Mylar, and durable outer layers such as gold. The layers are separated by thin netting to minimise conductivity. They are also often perforated to allow air to escape from the MLI after the spacecraft is deployed into space. As the number of layers increases, the effective radiation decreases. However, this relationship is not linear, and at a certain point, adding more layers no longer increases the insulation capability.

Typically, 25 layers are used.

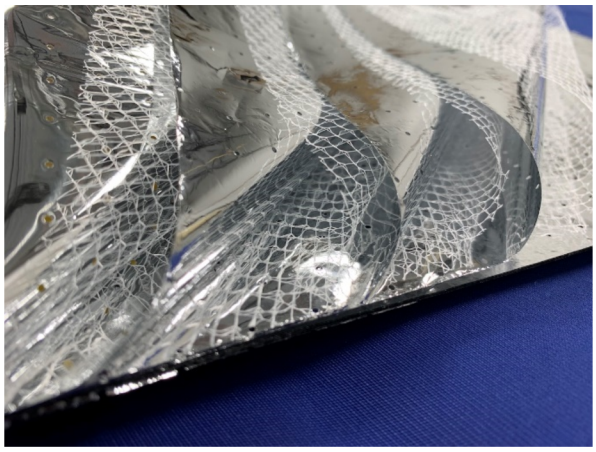

Fig. 4.2: Example of expanded MLI [22]

For CubeSats, MLI is not used as often because of the limited space available. They also increase the risk of getting stuck in the deployer, or there is a possibility that the layers will not stretch optimally and touch at some point, causing a short circuit that can significantly reduce the insulation capability.

Another area where insulation is applied is between individual components of spacecraft. In this instance, conductive insulators are utilised. These insulators operate on the same principle as resistors on a circuit board, whereby they add resistance to the thermal network. They are commonly employed as low-conductivity gaskets. In instances where the screw connection would have high conductivity, these insulators are placed between the individual components of the satellite or even between the screw and component, as can be observed in the Figure 4.3. This results in a reduction in the conductivity of the connection.[11][8][27]

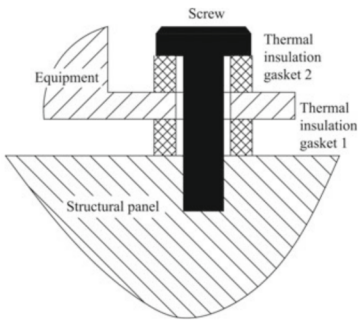

Fig. 4.3 : Schematic representation of application method of common thermal insulation gasket [8]

4.1.3 Thermal Straps

Thermal straps, sometimes called thermal links, are used to transfer heat between multiple locations. They are used, for example, when an electronic component overheats, and the surrounding structure is unable to dissipate all the heat on its own. Thermal straps are used as a thermal shortcut to the satellite's surface. They can be rigid or flexible, making them easy to apply mechanically. They are made of various materials, but the commonly used are copper and graphite.[19][26]

Fig. 4.4: Examples of thermal straps [20]

4.1.4 Thermal Radiators

The only way to reduce the temperature of the spacecraft is to radiate heat into space. This is done using a thermal radiator. These are areas on the surface of the satellite with high emissivity and low solar absorption. CubeSats usually have solar panels on each side and it is not possible to have a surface area for radiation. It is therefore more appropriate to use extendable radiators on them.[19][26]

4.1.5 Heat Pipes

Heat pipes are high thermal conductivity devices. They are used to transfer heat from one point to another. Unlike thermal straps, they can transfer heat more efficiently over longer distances with minimal heat loss. On the other hand, they are less effective when there is a small temperature gradient between the points. Heat pipes use the phenomenon of latent heat. The tubes have a porous, wicket-like structure. They contain a liquid at low pressure, close to its boiling point. As the liquid on one side of the pipe heats up, it begins to evaporate and move to the other end. At the cooler end, the vapour cools and condenses. It returns through the wick by capillary action. There are different types according to their conductivity: constant, varying and oscillating.[11][19][24]

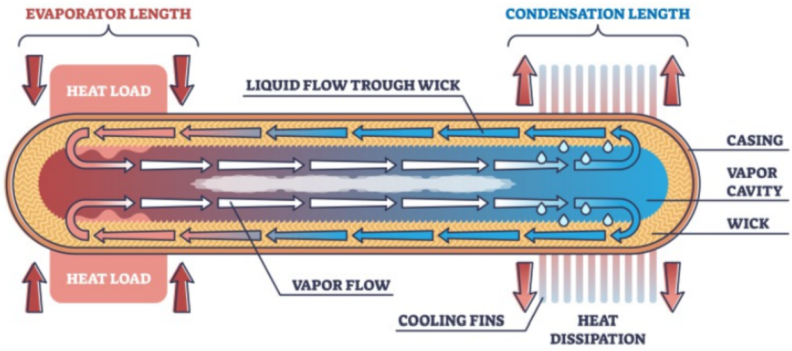

Fig. 4.5: Illustration of the operation of a heat pipe [24]

4.1.6 Phase Change Materials

Phase change materials (PCMs) store heat using latent heat. PCMs are placed in a metal case that is attached to the part of the satellite where a more stable temperature is required. As this location heats up, the PCM slowly changes state, usually from solid to liquid, while maintaining the same temperature. Conversely, as the location cools, the PCM releases heat as it begins to solidify. However, PCMs have a low thermal conductivity, so the metal casing must be highly conductive throughout its volume. Since PCMs are mostly paraffin, water, or glycerine, it depends on the temperature at which they need to be used, as we can see in the Table 4.1. The disadvantage of using them in CubeSats is the higher weight and volume requirements. [19][26]

Table 4.1: Reflectance values of various Earth surfaces [19]

Material	Melting Point (°C)	Heat of Fusion (kJ/kg)
Salicylic Acid	159	199
Bee Wax	61.8	177
Paraffin	20-60	140-280
Polyethylene glycol 600	20-25	146
Glycerol	18	199
Acetic acid	17	187
Water	0	333
Isopropyl alcohol	-89	88
Butane	-135	76
Ethane	-172	93
Methane	-183	59

4.2 Active Thermal Control Systems

Active thermal control systems are systems that actively manage the thermal state of various components. They use sensors to monitor the temperatures of the controlled parts, then evaluate their condition and adjust their heating or cooling as required. In contrast to passive systems, they are quicker to respond, more accurate and can maintain the temperature of components over a narrower band. Their main disadvantage is that they rely on electricity, so if there is a fault in the electrical system they can stop working. The most common are heaters, cryocoolers and fluid loops. While heaters are easy to implement in nanosatellites, other systems are difficult to integrate into them because their technologies have high space and mass requirements, so most of them are still in the development phase and have no flight heritage. So only a heater will be described. [11][26]

4.2.1 Heaters

There are several types of heaters, such as electrical resistance, radioisotope or chemical. For nanosatellites, the most suitable are electrical resistors in the form of patch heaters. Patch heaters, also called Kapton heaters, are made of polyamide film with an etched foil circuit. They are usually controlled by a thermostat or temperature sensor. They can have different shapes and wattages to suit a range of applications. They are commonly used to heat batteries as they have the narrowest operating temperature limits. They may fail over time, so it is recommended to have redundancy for long term use. [19][23]

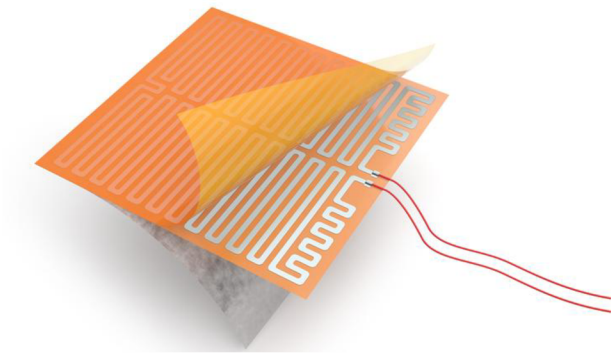

Fig. 4.6: Examples of patch heater [25]

5. THERMAL ANALYSIS

The objective of satellite thermal analysis is to predict the temperatures that the satellite will experience under specific or assumed environmental conditions. This analysis commences with the determination of the maximum and minimum temperatures that satellite components can withstand and the amount of heat they radiate. It is also important to define the temperature boundary conditions for each phase of the mission. These include the spacecraft's altitude and its orientation to the Sun and Earth. There are several software programs designed for this purpose. These are system programs that combine several common programs, including CAD programs, programs designed for standard thermal analysis, a program for mission analysis, and finally a computational program. The most commonly used programs are Thermal Desktop, ESATAN, or Systema Thermica. Thermica was chosen for this study.

5.1 Numerical Approximation Methods

The creation of an accurate analytical thermal model of even a very small satellite is currently impossible with the current state of knowledge and technologies. This is due to the complexity of the satellite itself, where there are different conductivities between components, jumps in materials, different sources and other inconsistencies that would require a huge number of equations. Therefore, numerical approximations are used to simplify the model to such an extent that it can be analysed even with less computing power, but at the same time it has sufficient accuracy and reliability. The fundamental principle underlying these methodologies is the decomposition of the model into discrete elements or nodes. The required parameters of the model are subsequently calculated within these nodes. The total number of nodes is dependent upon the size and complexity of the satellite, as well as the desired level of approximation accuracy. Conversely, it is important to consider that as the number of nodes increases, so too do the demands place upon the computer system. [28] [29]

5.1.1 Finite Element Method

The FEM discretizes the model into elements, with different shapes being used, though triangles or rectangles are the most common. Each of these elements has a node in each corner where required model parameters such as temperature are calculated. Based on the physical properties and boundary conditions of individual nodes, systems of equations are compiled. Techniques such as Euler's method or Runge-Kutta are used for calculation. This method was used by older versions of Thermica for simulations at instrumental

level. [8]

5.1.2 Finite Difference Method

FDM approximates the model directly using nodes. These nodes are located in the centre of the mesh, which is predefined and with its density the accuracy of the model increases. In each node, it represents the properties of one of the parts of the model. They are connected to each other using conduction and radiation heat transfer principles. The Taylor series is used to create a system of finite difference equations. Subsequently, these equations are converted to a series of algebraic equations, which are then solved using decomposition methods, iteration techniques, or matrix inversion schemes.[8] [28]

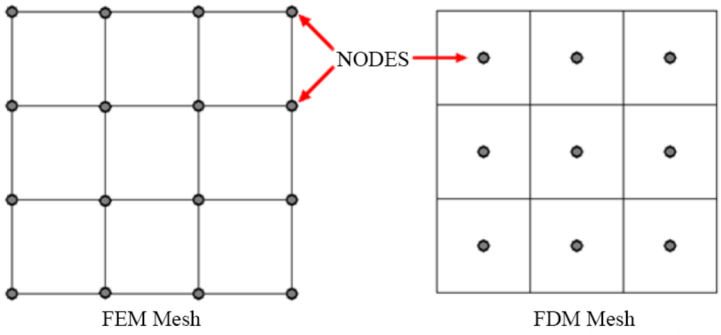

Fig. 5.1: Comparison of node organization in FEM and FDM [28]

5.1.3 Reduced Conductive Network

RCN is also known as the lumped-parameter method. Its principle is based on the analogy between the physics of heat and electricity propagation. It originated in the 1930s, at a time when computers were not yet available. It operated on the basis of individual points whose temperature capacity was adjusted by capacitors, while connections between nodes were adjusted by resistors. Subsequent developments led to the creation of numerical methods based on this principle. These are currently used in programs such as ESATAN or Thermica.

The lumped parameter method simplifies complex thermal systems by representing them with fewer components. Mathematically, it is analogous to using a simple formula to approximate more complex equations governing heat behaviour. For instance, instead of modelling every part of a machine, one might represent it as a single node that captures its overall heat capacity, connected by conductors to the rest of the system. This approach is useful when one does not require detailed knowledge of the temperature variations within the machine itself. [28] [29]

5.1.4 Monte Carlo Ray Tracing

The previous methods describe the propagation of heat by conduction or direct radiation. However, it should be noted that heat is also spread by the impact of reflected rays from individual parts of the satellite. These reflections are highly variable due to the heterogeneous nature of solid surfaces at the microscopic level. Consequently, it is essential to employ a statistical approach that accounts for the quasi-random nature of reflected rays. Monte Carlo simulation is therefore an appropriate methodology for this application, as it is a form of numerical analysis that is based on the generation of random values using usable stochastic data to generate approximate solutions. These random values are then employed in the ray tracing process itself, which is a mathematical model that describes the trajectory of photons within the system based on the physical interaction of photons with the surrounding environment. It accounts for absorption, reflectance, transparency and emission. [29] [30]

5.1.5 Steady State

In steady state thermal analysis, the thermal balance of a system is evaluated, wherein the temperature remains constant over time. Similarly, the heat flux entering and leaving the spaceship remains constant. This approach is employed to ascertain the temperature distribution of components within the system. This enables the identification of areas where components may overheat or act as heat sinks. Furthermore, a steady state serves as the foundation for transient analysis.[27]

5.1.6 Transient

In contrast to steady-state analysis, transient analysis examines the temporal evolution of the temperature of components in response to varying heat flux. In principle, a realistic and practical thermal design for satellites is based on this approach. It provides insight into how systems behave under dynamic conditions, enabling the design of systems that can withstand a variety of operating environments.[27]

5.2 Analysis of Extreme Cases

During the operational lifetime of the satellite, a number of factors can affect the temperature of the satellite, with the most significant being solar flux, albedo or component dissipation. It is also necessary to consider the lifetime of the mission, as the physical properties of surfaces and electrical components can change over time in orbit, which can substantially change the thermal behaviour of these components. Creating a model for the combination of all these parameters would be unnecessarily complex and

lengthy. For this reason, the most extreme cases of the mission are primarily investigated. The parameters used for these cases are selected so that the resulting thermal loads represent the most extreme cases that the satellite can experience during its mission. If the thermal management is able to maintain all components at their operating temperature even in these extreme cases, it can be assumed that it will be functional for the duration of the entire mission.

5.2.1 Hot Case

To conduct a hot case analysis, it is necessary to select parameters that will result in the satellite experiencing the highest possible temperature. This will involve a scenario with the highest possible solar constant. Therefore, it is essential to analyse the mission when the Earth is at its closest point to the sun, which occurs around 4th of January. Furthermore, it is important to consider when the components reach their highest dissipation. For instance, the on-board computer dissipates significantly more energy when it is processing data than when it is in standby mode. In the event that the mission is expected to last for several years, it is necessary to consider the impact of higher battery heating, as their capacity decreases. Furthermore, it is necessary to reduce the emissivity and increase the absorptivity of surfaces based on the results of previous experiments. [11]

5.2.2 Cold Case

Conversely, in the context of a cold case, it is imperative to consider the matter at the lowest possible temperature. Therefore, the mission must be calculated during the period when the Earth is furthest from the Sun, which is always around the 4th of July. In considering the magnitude of the dissipation, it is important to note that the value of zero should not be used as a baseline. Instead, the minimum possible values should be employed when the satellite is still in functional mode, such as in the safety mode. [11]

6. MISSION CIMER

CIMER (Cyanobacteria In Microgravity Environment Research) is a 3U CubeSat student bio-mission which aims to investigate the potential benefits of desiccative hibernation for cultivating biological substances in space. This mission was created in collaboration between Brno University of Technology and Mendel University. The results of this mission could help us to gain a deeper understanding of the bio-cultivation process and to test technologies that will be used for cultivation on more complex systems in the near future. This mission is still in development, which includes the thermal design itself in this work.

6.1 System Architecture

The following paragraphs provide an overview of the principal subsystems of a satellite. These subsystems are responsible for various functions essential for the proper functioning of the satellite and play a vital role in its design and operation. A redundancy of critical components, such as the payload OBC, was incorporated into the system design.

6.1.1 Payload MIBICO

The primary objective of this mission is to transport MIBICO, a 1.5U unit equipped with four microbiological containers, each measuring 20x20x40 mm, designed to house cyanobacteria. These containers are hermetically sealed to protect their contents from the harsh conditions of space. MIBICO is equipped with sensors to monitor oxygen levels, humidity and radiation to provide the controlled environment necessary for the biological experiment. Each container contains small cuvettes filled with moistened sponge with bacteria. Sponge is very important to keep water in uniform distribution in microgravity.

The experimental design requires strict control of temperature and light to mimic the natural circadian rhythms of the cyanobacteria found on Earth. To achieve this, the bacteria are subjected to a light cycle of 12 hours of light followed by 12 hours of darkness every 24 hours, facilitated by two LEDs per container. The temperature is maintained at approximately 22°C, with allowed variations limited to ±3°C.

The bacteria are desiccated before being placed in the containers. They are kept in this state until the start of the actual experiment, when they are hydrated and then cultured at the specified temperatures and light cycles. This will enable them to survive the harsh conditions during the launch and subsequent deployment of the satellite into orbit, when they will experience extreme temperature fluctuations.

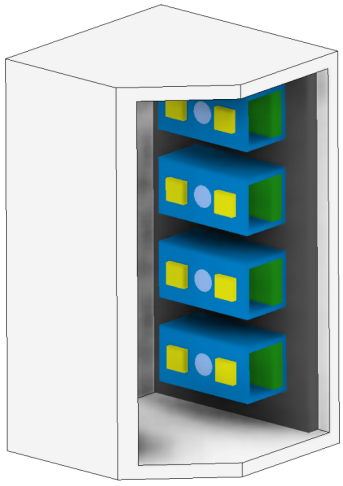

Fig. 6.1: Schematic representation of MIBICO. Blue boxes represent containers, cuvettes with cyanobacteria are marked in green and yellow squares are LEDs

6.1.2 Payload OBC

The secondary payload for this mission is a payload on-board computer (POBC) specially designed to operate in the harsh conditions of space. This POBC will be used to monitor and execute the biological experiment. It is still under development, but basic parameters have been defined. It will be designed to conform to the PC104 standard, ensuring compatibility with a wide range of existing CubeSat systems. The specifications for the OBC state that its dimensions must not exceed 96x96x20 mm and its mass must be less than 200 grams. Power consumption during computational activities is limited to a maximum of 4 watts.

6.1.3 Electrical Power System

The Electrical Power System (EPS) is a critical subsystem in satellites, tasked with managing and distributing electrical energy. This system is composed of solar panels, batteries, and a system board.

In the CubeSat CIMER, the primary power source is a set of 12 solar panels supplied by Spacemanic. These are high-efficiency triple-junction GaAs panels, which provide an average output of 2.3 W per panel in low Earth orbit with a conversion efficiency of 30%.

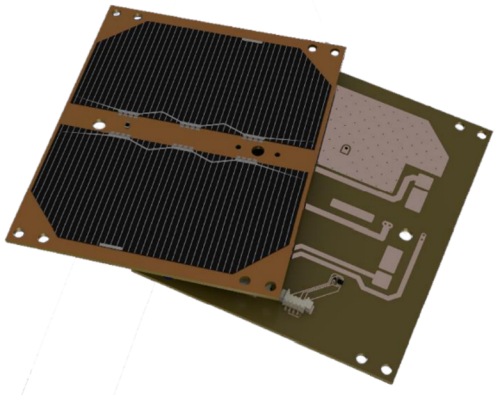

Fig. 6.2: Spacemanic solar panels [32]

The batteries play a vital role in maintaining satellite operations during periods when the CubeSat passes into the Earth's shadow, and the solar panels are inactive. Additionally, batteries help in regulating and distributing power throughout the satellite. The CubeSat CIMER utilizes a Li-ion 18650 battery pack from Innovative Solutions In Space (ISIS), comprising four batteries housed within a specially designed case that can be mounted directly onto the satellite's rails. This design includes built-in temperature sensors and heat strap to manage thermal fluctuations. The batteries operate within a broad temperature range, although their efficiency decreases during charging and discharging cycles, which requires careful thermal management.

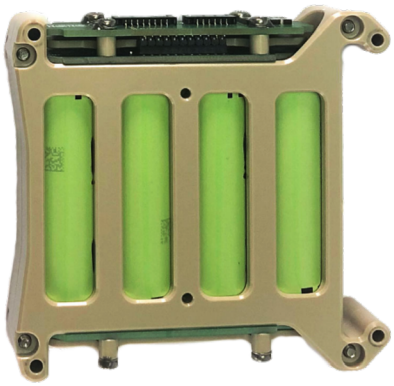

Fig. 6.3: ISIS battery pack [33]

ISIS also provides a direct control unit for the EPS, designed to regulate the voltage from the solar panels and the output from the batteries. This ensures that the batteries are

protected from damage due to high power consumption or rapid charging rates. Moreover, this unit acts as a voltage regulator between the battery output and other satellite interfaces, enhancing the overall reliability and stability of the power supply system. [28] [29] [30]

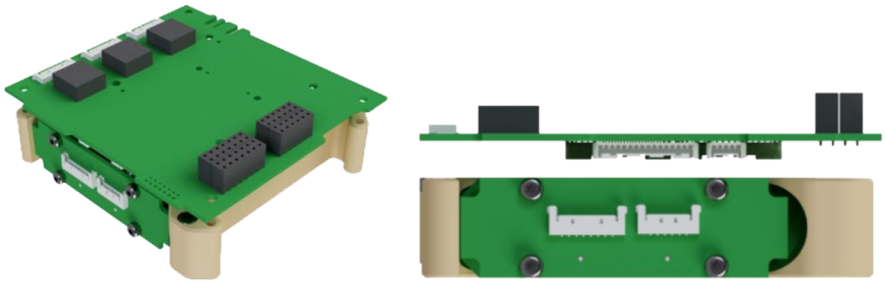

Fig. 6.4: Arrangement of control unit of EPS and battery pack [33]

6.1.4 OBC

The on-board computer (OBC) is responsible for ensuring the optimal progression of the mission. The device contains the primary microcontroller, memory, and communication interface. It is responsible for the collection of data from the payload or response command, which is referred to as telemetry. The OBC employed by Spacemanic Eddie will be utilised for the CIMER. The computer is designed to be easily installed and configured, with a built-in gyroscope, magnetic and temperature sensor. The implementation on the PC 104 board is straightforward. [28] [29]

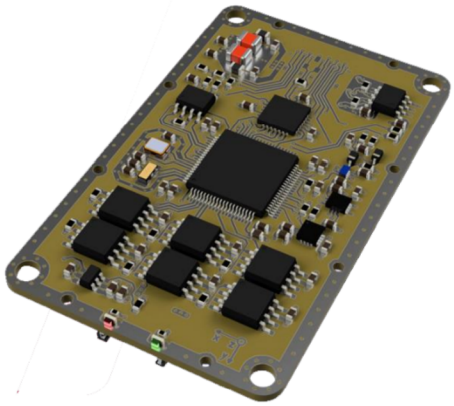

Fig. 6.5: Spacemanic OBC Eddie [32]

6.1.5 Communication System

The communication system (COMs) for CubeSat missions comprises a receiver/transmitter setup, an antenna on the satellite, and a ground station. Typically, CubeSats utilize VHF radio bands at 145 MHz and UHF at 435 MHz for communication. For high data volume transmissions, higher frequency bands are also employed.

The proposed communication system for CIMER will utilize a custom-built university VHF/UHF ground station, which is designed for both downlink and uplink communication with a satellite on LEO. It is also considered collaborations with other academic institutions to enhance our communication system's signal coverage. This expansion would involve a network of UHF ground stations situated at various universities, enabling broader communication coverage with the satellite.

To ensure redundancy, our satellite will be equipped with two low-power UHF/VHF transceivers from Spacemanic. These transceivers, named Murgas, are modular and compatible with the standard PC 104 stack, allowing two units to be mounted on a single board. In normal operations, one unit will function solely as a receiver, while the other will serve as a transceiver. This configuration is anticipated to facilitate the transmission of scientific measurements and telemetry data at sufficient data rates.

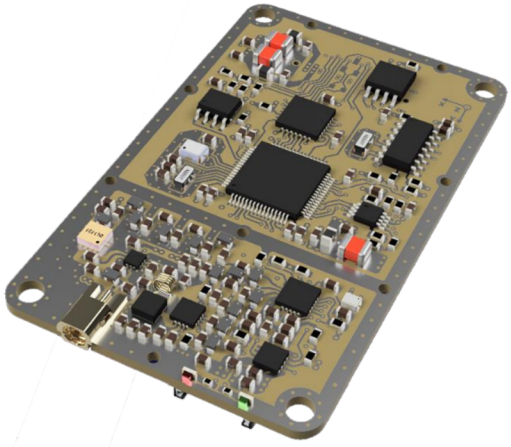

Fig. 6.6: Spacemanic transceiver Murgas [32]

The satellite's antennas must achieve an optimal balance between gain and beamwidth to minimise the necessity for adjustments by the Attitude Control System (ACS). A deployable antenna system from ISIS, comprising four spring-loaded antennas, will be employed. These can be configured in pairs, with two antennas dedicated to the VHF band, measuring 17 cm in length, and two for the UHF band, each 55 cm long. This arrangement ensures efficient management of space and operational flexibility. [31] [32] [33]

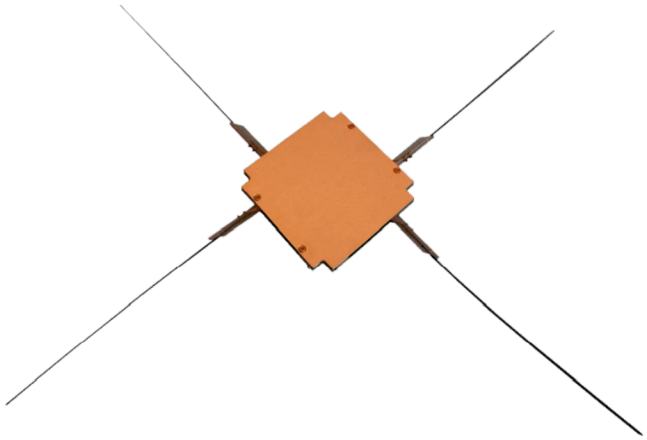

Fig. 6.7: ISIS deployable antenna [33]

6.1.6 Attitude Control System

The payload of this mission is not subject to any requirements regarding the position and rotation of the satellite. Furthermore, the use of a high beamwidth antenna allows for the elimination of any device for position control. The satellite will contain only a small magnet that will ensure its alignment with the Earth's magnetic field. This will prevent excessive spin in any axis and permit slow rotation according to the changing magnetic field of the Earth during the orbit. There is also no strict request for orbit in this mission So the most frequently used orbit for share ride sun-synchronous orbit with an altitude of 500-600 km will be used.

7. THERMAL MODELLING OF CUBESAT CIMER

This chapter will describe the process of creating the CIMER CubeSat thermal model. The model was created using the Systema Thermica software developed by Airbus Defence and Space.

7.1 Basic principles of Thermal Modelling

As previously stated, the mathematical methods employed for thermal model analysis are computationally demanding when the model contains excessive detail. Consequently, thermal models are simplified in comparison to standard CAD models. The majority of models utilise surfaces with assigned thicknesses as their properties. This approach enables significant acceleration of calculation times while maintaining the requisite accuracy. The Figure 7.1 illustrates the manner in which a component can be simplified. The original shape of the bracket is shown on the left. This model would use up to 415 nodes in a standard analysis, but in a thermal analysis only 2 nodes may be sufficient since it is a direct body that conducts heat from one end to the other.

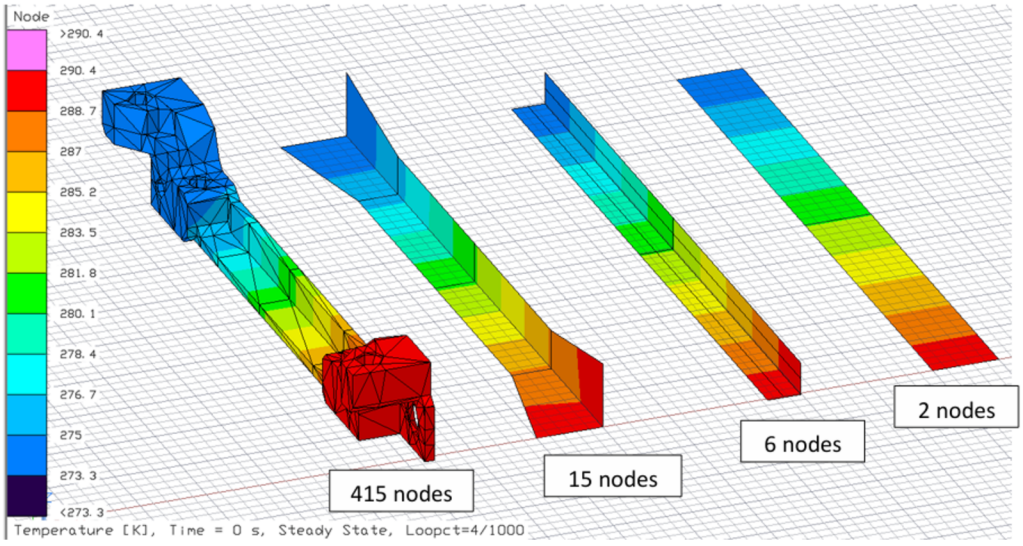

Fig. 7.1: Thermal design of bracket [26]

However, when simplifying the model in this way, it is essential to consider the basic physical properties of the components, especially the mass. Thus, if the shape of a component is simplified, it is necessary to give it a thickness such that the final mass is the same before and after unification. In this way, the whole model must be simplified. The recommended number of nodes for a CubeSat of size 3U is 500 to 1000 nodes. It

should be noted, that this recommended value is only a guideline, and that the number of nodes required for a given spacecraft will depend on its complexity.

Modelling bolted joints in the model is unnecessary; furthermore, the individual components do not need to be in contact with each other. All these connections are added to the program as conductive couples or surface contacts are added to the program, and then their respective value is entered. In this manner, connections with wires can also be added, which on occasion require consideration.

It can be challenging to estimate the thermal conductivity between any two surfaces. In such instances, estimated values are employed, with the objective of determining the influence of variations in thermal conductivity on the temperature profiles of surrounding components over time. In the event that these changes are highly sensitive to variations in thermal conductivity, it is recommended that the joint undergo further investigation.

7.2 Thermal Model in Systema Thermica

The following subsections will describe the thermal and material properties of all subsystems in detail. The majority of the thermo-optical properties of the materials were obtained from MatWeb [34] and other papers focusing on this issue, with the remainder calculated by averaging. At the time of this work, the satellite itself was still in design, so some materials and components may differ slightly from the final design.

7.2.1 Structure

The structure is constructed from aluminium 6061. As can be observed in the figure, the structure has been simplified to a significant extent. In order to maintain its weight and, consequently, its thermal capacity, the average thickness of the individual components was selected to be 2.5 mm. M3-sized screws were employed to connect the disparate components of the structure, as well as throughout the remainder of the model. The conductivity of the joints was set to 0.26 W/K, in accordance with the findings of [23]. It is also necessary to consider the thermal conductivity of the surfaces of the individual parts in contact with one another. It is assumed that these contacts will be functional, and thus a suitable surface treatment will be applied in these areas. From the standpoint of engineering practice, such contacts are typically assigned a conductivity of approximately 2000 $W.K^{-1}.m^{-2}$.

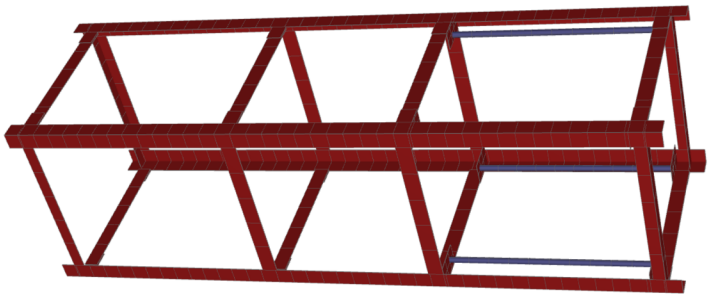

Fig. 7.2: Thermal model of structure

7.2.2 Printed Circuit Boards

The fundamental components of all electronic subsystems are printed circuit boards (PCBs). These are primarily composed of layers of copper alternating with an FR4 insulator. The precise thermal conductivity of a PCB is not readily ascertainable, as each one is developed in a unique manner and possesses distinct conductive pathways. Consequently, the majority of calculations are based on average values. In this work, PCBs are considered with a 1.6mm thickness and eight copper layers. The average conductivity is 20.5 $W.m^{-1}K^{-1}$, the density is 2223 $Kg.m^{-3}$ and the specific heat is 589 $J.kg^{-1}.K^{-1}$. [32]

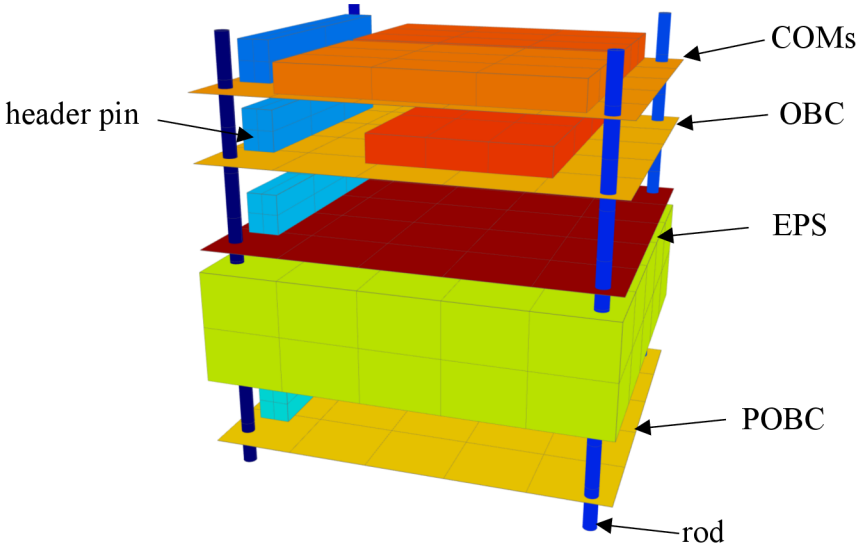

Fig. 7.3: Representation of PCB arrangement in thermal models

As can be seen in the Figure 7.3, all the electrical components are interconnected with each other using header pins. The conductivity of the pins was calculated by averaging the properties of the materials that comprise them. The pins are composed of a base material, with the ratio of the cross-sectional area determining their composition. The pins themselves are made of a gold-tin alloy and are isolated using a PBT polymer. The values used and calculated can be seen in the attached table. The conductivity between the header pin and the PCB has been considered as 1 $W.K^{-1}$ based on [35] [36]

Table 7.1: Thermal properties of header pin [34]

	Area [mm^2]	Density [kg/m^3]	Conductivity [$W.m^{-1}.K^{-1}$]	Specific heat [$J.kg^{-1}.K^{-1}$]
Au Sn	72.94	14510	57	150
PBT	577.06	1300	0.21	1210
Overall	650	2782.36	6.58	1091.05

The thermal properties calculated in the table are valid only in the z-axis direction. It is not necessary to consider the properties in the x-y plane, as there is no heat propagation in the pins in these directions.

Further thermal coupling between the subsystems is created by the threaded rods on which they are attached. The thermal conductivity of this joint has been considered to be 0.1 $W.K^{-1}$. [35]

7.2.3 Communications system

The Figure 7.4 depicts a simplified model of PC104, comprising modules for transceiver (TX) and receiver (RX). The modules themselves have been simplified to simple boards with the same features as the other PCBs, but with higher thicknesses to preserve the original module weight. Additionally, they are provided with covers. These covers are manufactured from aluminium and serve a protective function. The conductivity between the modules and the PC104 has been set to 5 $W.K^{-1}$.

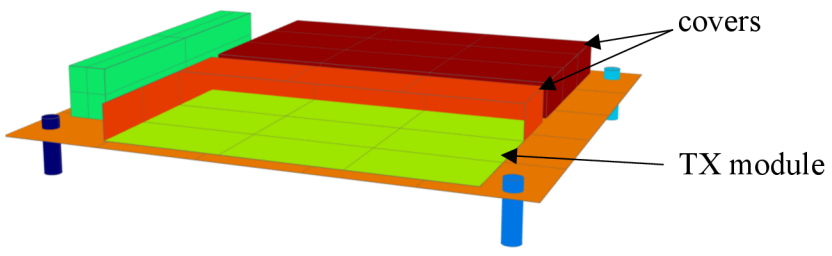

Fig. 7.4: Thermal model of TX and RX module

In addition to the header pins and rods, this board is also thermally connected to the antenna with a coaxial cable. The conductivity of this connection was calculated from the cross-sectional area of the copper component of the cable, given that the dielectric can be considered a perfect insulator, the estimated length and conductivity of the copper can be seen in Table 7.2. These values were determined for a coaxial cable of type RG58 C/U.

Table 7.2: Parameters of coaxial cable of type RG58 C/U [37]

a [mm]	**b [mm]**	**c [mm]**	**Length L [mm]**	**Conductivity k Cu [$W.m^{-1}.K^{-1}$]**	**Area A [mm^2]**
0.508	2	2.2	30	385	3.45

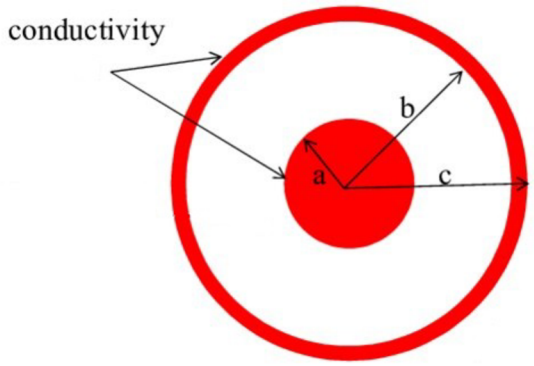

Fig. 1.5: Cross-section of coaxial cable [37]

$$C = \frac{kA}{L} = \frac{385*3.45*10^{-6}}{30*10^{-3}} = 0.044\ W \cdot K^{-1} \tag{7.1}$$

The remaining driver connections were evaluated using a similar procedure. However, as can be seen with the coaxial, which has the largest cross-section, its thermal conductivity is quite low, so some other thermal connections via wires have been neglected.

The antenna was constructed as a simple rectangular box, with the bottom part comprising a PCB with a thickness of 1 mm on which the spring antennas were placed. These were excluded from the model, given their small cross-section and area, and the negligible effect they would have on the overall temperature of the structure. The top of this is covered by an aluminium plate of a thickness of 0.8 mm, which can be observed in the accompanying Figure 7.6. The antenna was presented in an inverted position in order to facilitate better visualisation.

The communication system will operate in two distinct modes, namely transmitting and receiving. During the transmission phase, the thermal dissipation at the transmitter will be 1 W, while during the reception phase, it will be 0.1 W.

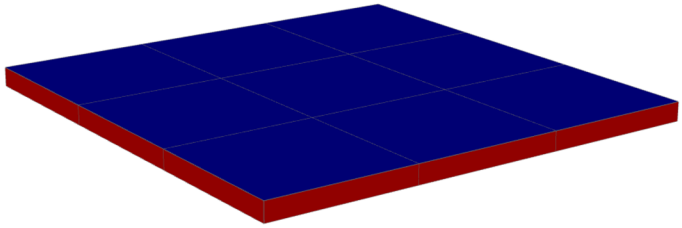

Fig. 7.6: Thermal model of ISIS deployable antenna

7.2.4 OBC

The OBC is designed in a similar manner to the receiver and transmitter. The module is also represented by a rectangle with PCB material features and a thickness calculated to fit the weight. The same principle applies to the aluminium housing.

Two modes will be considered for the OBC: a process mode, in which data from the POBC is processed and sent, and a standby mode. For the first case, the dissipation will be 1 W, while for the second case, it will be 0.1 W.

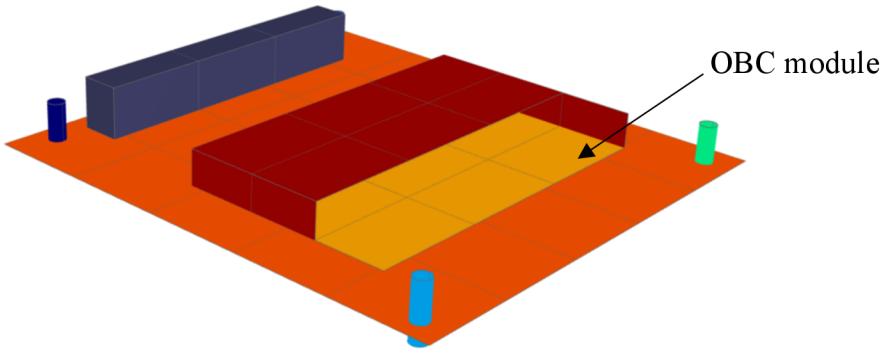

Fig. 7.7: Thermal model of on-board computer

7.2.5 EPS

As illustrated in the Figure 7.8, the plastic packaging of the batteries has been simplified to a simple block, while the batteries themselves have been reduced to a rectangle with a thickness of 14 mm. While ISIS does not specify the exact material of the plastic packaging, polyether ether ketone (PEEK) has been considered as the standard thermoplastic used in space applications. One side of the packaging is designed to accommodate a PCB, to which the batteries are conductively connected with a value of 2 $W.K^{-1}$ per battery. This PCB is further thermally coupled to an EPS module, which is modelled on the previous PCB as other subsystems. The conductivity of this junction was set to 0.1 W.

The internal dissipation of the battery is quite small. During charging and discharging, it has a value of 0.1 W. Outside of these processes, batteries do not dissipate. The EPS module has a thermal dissipation of 1 W at maximum load.

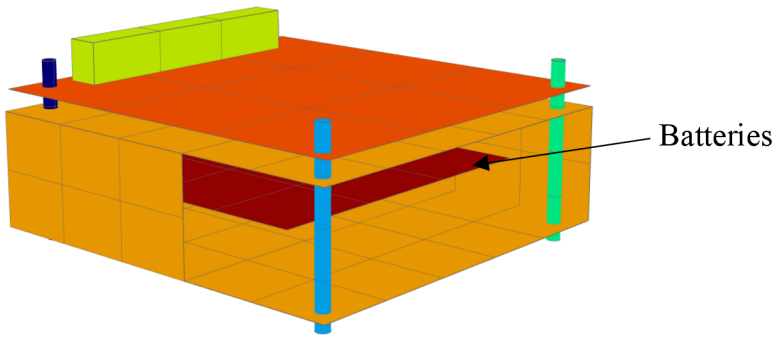

Fig. 7.8: Thermal model of electrical power system

Given that aluminium 6061 constitutes the overwhelming majority of the volume of solar panels, the thermo-physical properties of these panels were determined in accordance with the properties of this metal. The model was simplified to a series of simple rectangles. However, it is necessary to consider the different surface properties. Thus, the exterior of the panels exhibits an emissivity of 0.52 and an absorptivity of 0.42, while the interior properties remain consistent with those of other aluminium components.

The solar panels are attached to the structure with screws, which are incorporated into the model as thermal couplings. Additionally, surface contact is considered, which is assumed to be of lower quality in this case, and thus assigned a value of 1000 $W.K^{-1}.m^{-2}$.

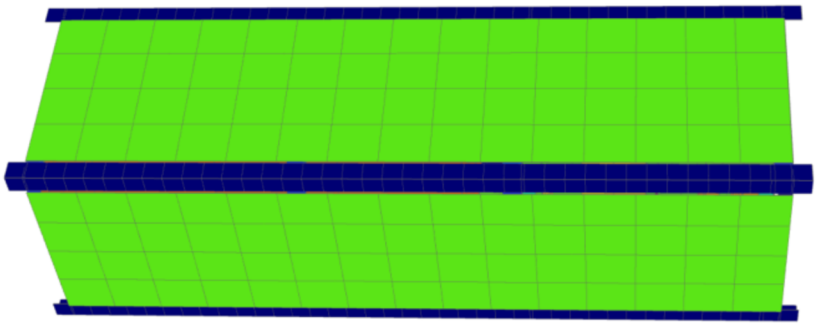

Fig. 7.9: Thermal model of solar panels

7.2.6 Payload OBC

As the POBC is still under development, it was not possible to specify its properties and shape. Consequently, the POBC is represented by a simple PCB with an assumed thermal dissipation of 4 W at maximum power and during data processing from the experiment. The second mode will be in a standby state, analogous to the OBC mode with a dissipation of 0.1 W.

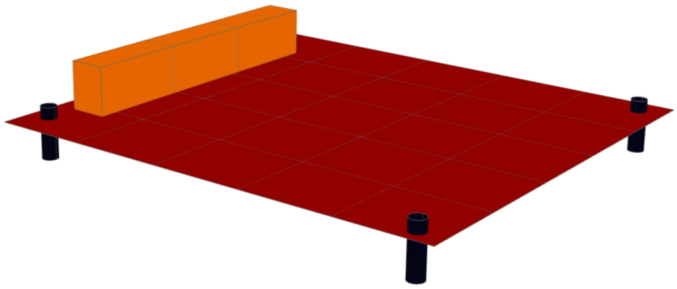

Fig. 7.10: Thermal model of payload OBC

7.2.7 MIBICO

The creation of a thermal model for the experiment itself represents the most crucial aspect of this work. As part of this process, the design is also included. Therefore, during the initial creation, a simple model was developed to determine the thermal parameters that occur, and it will be subsequently adjusted in further iterations. The outer casing of the CubeSat is made of 0.3 mm thick aluminium 6061, which is attached to the structure with four ribs using screws.

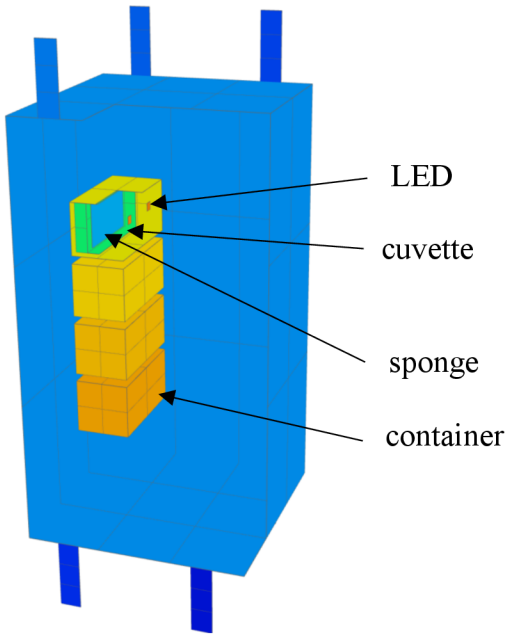

Fig. 7.11: Thermal model of MIBICO

In the original design, the POBC was supposed to be part of the outer casing itself, but it had to be moved outside because, during its peak activity, it overheated the entire casing, and the temperatures of the bacteria significantly exceeded the limits. Inside the casing, there are four hermetically sealed containers also made of 6061 aluminium, which are screwed onto the back side of the outer casing. Inside these containers are cuvettes made of PMMA. The cuvettes contain moistened sponges, whose properties are averaged between the properties of water and natural rubber in a 50-50 ratio. Sponge is made from natural rubber.

Table 7.3: Thermal properties of natural rubber and water [39]

	Density [kg.m^{-3}]	**Conductivity [W.m^{-1}.K^{-1}]**	**Specific heat [J.kg^{-1}.K^{-1}]**
Natural rubber	930	0.14	0.45
Water	1000	0.6	4180
Whole	965	0.37	2090.225

The initial physical values are considered at room temperature, as this is the temperature at which the goal is to maintain conditions. The conductive contact between the containers and the casing was set to the most unfavourable scenario for the contact of two aluminium plates in order to achieve the greatest possible insulation of the containers from the surrounding environment. This type of contact can have a conductivity of 500 W.K^{-1}.m^{-2}. The contact between the cuvette and the container was assigned the same

value. It may be assumed that a high quality of contact will be achieved between the sponge and the cuvette because water adheres well to the cuvette's walls. Cuvettes are transparent so there is no need to set optical properties to them.

Each container also contains two diodes, each with a thermal dissipation of 0.2 W when illuminated. Other sensors were excluded from the model due to their limited size and negligible thermal dissipation.

7.2.8 Model Property Summary

The total number of nodes distributed across the model is 1670, which is slightly above the recommended threshold. The number of nodes is higher than the recommended amount in order to achieve the highest accuracy. At the current quantity, the calculation time on a desktop device is approximately five minutes, which allows for the use of more points. The Figure 7.12 depicts the complete CIMMER term model.

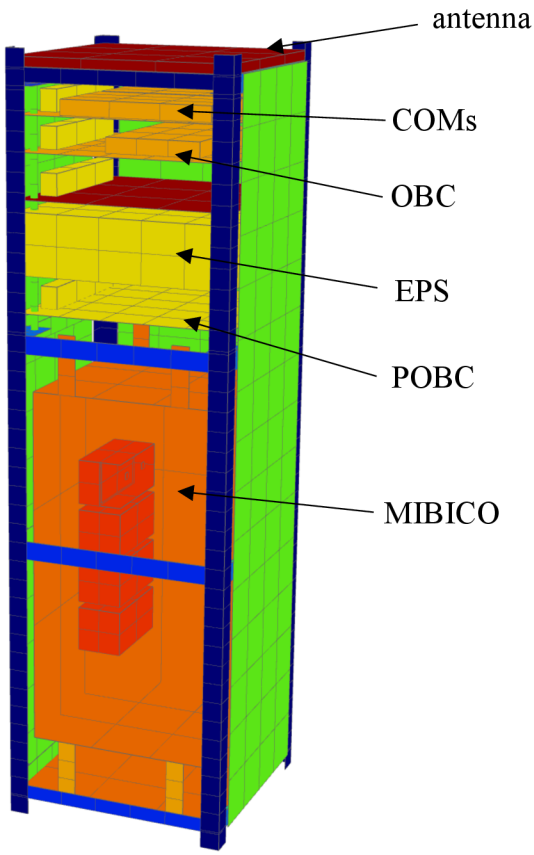

Fig. 7.12: Thermal model of MIBICO

The following tables will provide a comprehensive overview of the essential properties of the materials and joints included in the thermal model:

Table 7.4: Thermophysical properties

Material	Conductivity k [$W.m^{-1}.K^{-1}$]	Heat capacity c_p [$J.Kg^{-1}.K^{-1}$]	Density ρ [$kg.m^{-3}$]	Reference
Aluminium 6061	167	896	2700	[40]
Li-ion Batteries	15	953	2700	[41]
PEEK	0.25	1320	1700	[26]
PCB	18.04	1544	2259	[26]
Copper	398	385	8960	[42]
PMMA	0.19	1470	1190	[43]
Pin header (lumped)	3.41	1150	2045	
Sponge with water (lumped)	0.37	2090	965	

Given that the anticipated duration of the mission is six months, it is not necessary to consider the potential changes in optical properties during the mission. Only the beginning of life (BOL) properties have been taken into account.

Table 7.5: Optical properties

Component/Material	emissivity ε [-]	absorptivity a [-]	Reference
Aluminium 6061	0.03	0.16	[26]
Solar panels	0.86	0.6	[35]
PCB	0.9	0.81	[35]

The following table presents the conductivity values between the two surfaces.

Table 7.6: Surface contacts quality

Component 1	Component 2	Surface contact quality Conduction [$W/K/m^2$]
Structure	Structure	2000
Structure	Solar panels	1000
Structure	MIBICO case	2000
MIBICO case	Containers	500
Container	Cuvettes	500
Cuvettes	sponge	2000
Container	Containers	2000

The final table provides an overview of the thermal conductivity connections between the individual components.

Table 7.7: Conductive couplings [26][35]

Component 1	Component 2	Conductance [W/K]
Screws	Structure, MIBICO, Solar panels	0.26
Pin Header	PCB	1
OBC	PCB	5
TX	PCB	5
RX	PCB	5
rods	PCB	0.26
PCB	Antenna	0.044
Batteries	PCB	2
PCB	EPS	0.1

7.3 Thermal model analysis

A sun-synchronous orbit with an altitude of 500 km. It is estimated that one simulation will require 15 orbits to sufficiently stabilise all component temperatures. Satellite will always point in the direction of the North Pole, rotating around its own axis. The model will be analysed in two distinct modes: namely, Cold case and Hot case. The following chapters will describe the modes and ranks that will be computed in these two cases.

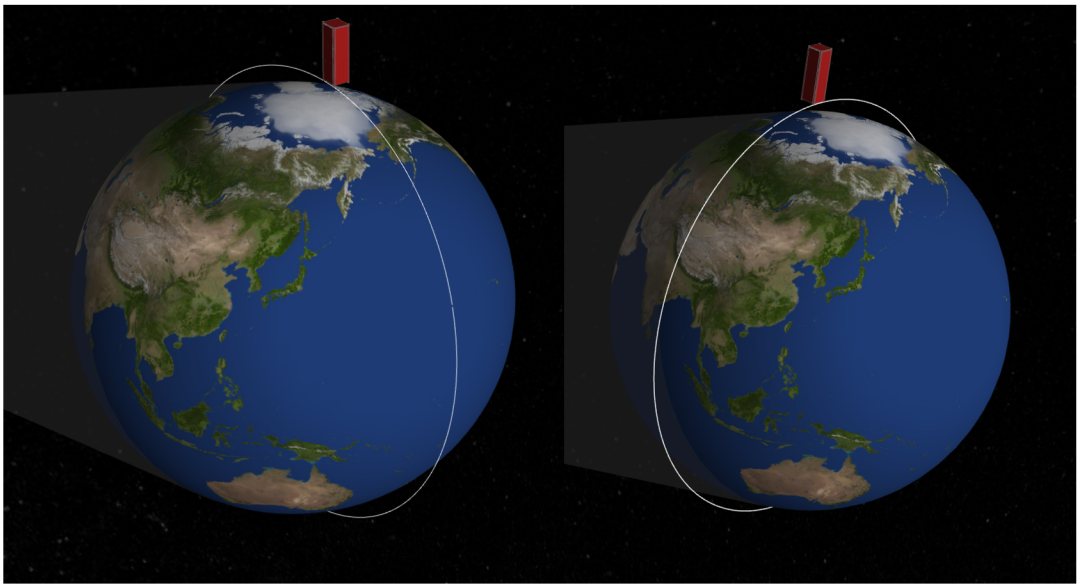

Fig. 7.13: Visualization of orbits for Cold case on the left and Hot case on the right

7.4 Cold Case

In the context of cold case analysis, the analysis date will be set to 4th of June which corresponds to the date when the sun is at its farthest distance from the Earth. The LTAN will be set to 00:00:00, which represents the state when the satellite spends the longest period of time in the Earth's shadow. The Earth's infrared radiation is set to 227 W/m^2, and the albedo is set to 0.15. The attached table provides a listing of the internal dissipation rates during the cold case.

Table 7.8: Cold case heat dissipation

	Heat dissipation [W]
TX	0
RX	0.1
OBC	0.1
EPS module	1
Batteries	0
POBC	0.01
LED	0

7.4.1 Hot case

A hot case analysis will be conducted at 4:1:00 a.m. on the day of the year when the Earth is at its closest point to the Sun. The LTAN will be 00:00:00 when the satellite will experience the least amount of shadow during its orbit. The Earth's infrared radiation is 265 W/m^2, while its albedo is 0.3. The table below presents the dissipation values.

Table 7.9: Hot case heat dissipation

	Heat dissipation [W]
TX	1
RX	0.1
OBC	1
EPS module	1
Batteries	0,1
POBC	4
LED	0,2

7.5 Analysis results

This chapter will present the results of the preliminary analysis of the model, which was created based on previous parameters.

7.5.1 Cold case analysis

In the case of the cold case, the temperatures of all subsystems are within the specified operating temperature ranges, with the exception of the MIBICO payload and to a lesser extent the batteries. The batteries are partially outside of the specified limits, although they have a lower low temperature limit in this case compared to the hot case, due to the assumption that these minimum values will be reached mainly when the satellite is in shadow, and thus the batteries will be in discharge mode. However, the image indicates that the temperature does not rise sufficiently high during the entire simulation period for charging to begin. This problem is solved by a heater, which is directly implemented in the battery casing. Therefore, it is likely that the satellite will need to use it at certain phases of its mission.

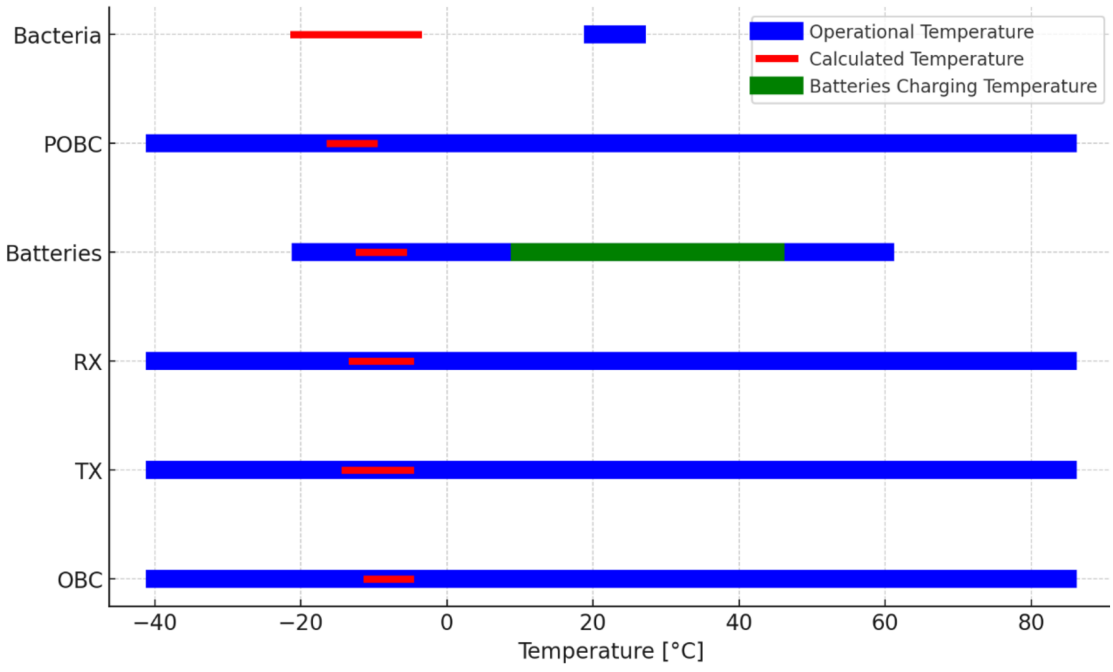

Fig. 7.14: Comparison of operational and calculated temperatures for Cold case

Table 7.10: Temperatures of subsystem for Cold case

	Operational temperatures [C°]		Calculated temperatures [C°]	
	Min.	Max.	Min.	Max.
OBC	-40	85	-11	-5
TX	-40	85	-14	-5
RX	-40	85	-13	-5
Batteries	-20	45	-12	-6
POBC	-40	85	-16	-10
Bacteria	20	26	-21	-4

In the case of MIBICO, it can be observed that the current temperatures do not meet the requirements at all. Consequently, it is necessary to make changes to the architecture of this container. It is evident that a heater will be required, as the temperatures do not even reach the minimum required temperature. Furthermore, it is necessary to improve the insulation of the containers in order to reduce temperature fluctuations.

7.5.2 Hot Case Analysis

The results of the hot case analysis indicate that, in this instance, all subsystems are within the required operational temperature parameters, with the exception of the payload. In this case, the temperatures of the cyanobacteria rise well above the set limit. Analysis of the model shows that this is caused by the payload OBC, which, at its maximum activity, heats up its surroundings and thus the payload itself.

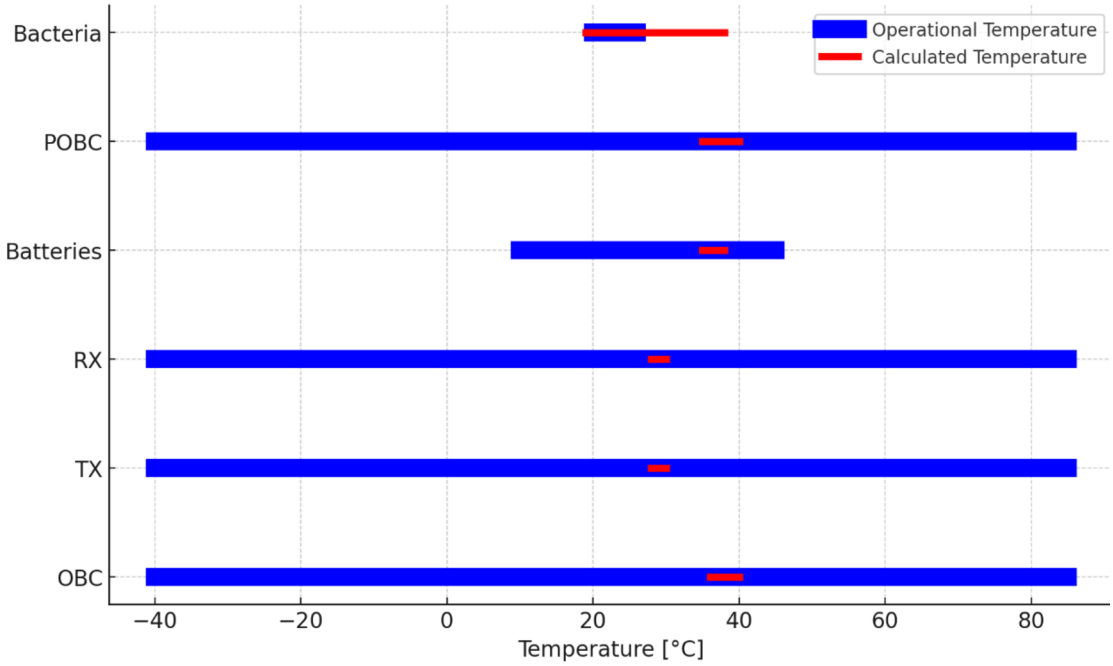

Fig. 7.15: Comparison of operational and calculated temperatures for Hot case

Table 7.11: Temperatures of subsystem for Hot case

	Operational temperatures [C˚]		Calculated temperatures [C˚]	
	Min.	**Max.**	**Min.**	**Max.**
OBC	-40	85	36	40
TRX	-40	85	28	30
RX	-40	85	28	30
Batteries	10	45	35	38
POBC	-40	85	35	40
Bacteria	20	26	19	38

When the LEDs are operational, the batteries have reached a sufficient temperature, therefore, the use of a heater to warm them is not necessary in that moment. However, it is necessary to insulate the container to reduce temperature fluctuations.

7.5.3 Conclusion

There are several reasons why almost all temperatures are within their specified limits. The optimal altitude of the CubeSat allows it to be sufficiently warmed by the Earth, even when in shadow. The satellite rotates slowly around its axis, effectively "grilling" itself and warming up from all sides during its orbit. The electrical subsystems are arranged in

a compact configuration, which helps to maintain a stable temperature.

However, the cyanobacteria themselves have much stricter temperature limits than the other components, so the payload design must be adapted to keep the temperature of the cyanobacteria within the specified limits.

7.6 Thermal design of CubeSat CIMER

The following chapter will describe the process of designing the payload and its surroundings in order to ensure that they meet the required temperature limits.

7.6.1 Overheating

As can be seen on Figure 7.16, the overheating of the cyanobacteria is mainly caused by the high power consumption of the payload OBC. This overheating can be solved by using a thermal strip, which is attached from the bottom of the PCB to the side where it heats up the most, and the other side is attached to the inside of the solar panel. In this way, the heat is transferred directly to the surface of the satellite, where it is then radiated into space.

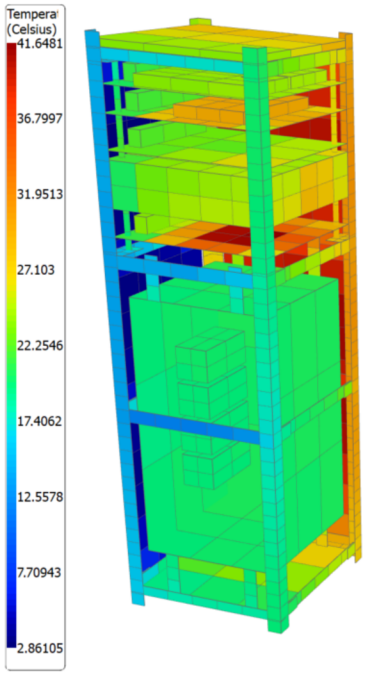

Fig. 7.16: Thermal model of MIBICO

Further simulations showed that the thermal strip needed to be able to transfer 0.8 W/K of heat. From this value and the thermophysical properties of copper, which is the

most commonly used material, the required cross-section of this strip was then calculated, as shown in the following equations. The length of the strip was estimated to be 70 mm.

Table 7.12: Values for estimating of area of thermal strap [41]

Length L [mm]	Conductivity k Cu [W/m/K]	C [W/K]
70	385	0.8

$$C = \frac{kA}{L} => A = \frac{Cl}{k} \tag{7.2}$$

$$A = \frac{0.8 \cdot 0.07}{385} = 1.45 \cdot 10^{-4} m^2 = 1.45 cm^2 \tag{7.3}$$

7.6.2 High temperature fluctuations

A further limitation of the previous model was the high temperature fluctuations that could potentially be lethal to the cyanobacteria. These were addressed through two distinct approaches. Firstly, by improving the insulation of the containers within the main package, thereby preventing their temperature from being reflected by every temperature fluctuation in the model. Secondly, by increasing the thickness of the walls and incorporating additional material to enhance the thermal inertia of the containers.

The material was augmented by increasing the thickness of the walls of the containers to 1 cm. Furthermore, a block of aluminium with dimensions of 12x6x2 cm was incorporated into the front wall, which serves as a heat reservoir and thus mitigates rapid temperature fluctuations. Aluminium was selected due to its optimal ratio between density and heat capacity among the materials employed in the space industry, while also offering a relatively low cost. To ascertain the feasibility of inserting the aforementioned block of aluminium into the experiment, a mass budget was calculated for verification purposes. This is presented in the table below. The maximum mass for a 3U CubeSat is 4000 grams. With the dimensions selected, there should be sufficient space for the other components in the experiment.

Table 7.13: Mass budget for Cimer

Subsystem	Component	Mass [g]
OBC	OBC PCB	25
EPS	EPS	360
	Solar panels	600
COMS	COMS modules	50
	UHF/VHF antenna	100
MIBICO	Structure	6.7
	Container	1833
	Hermetic boxes	108
	Cuvettes	24
	Sponge with water	30
	PC controller	25
	Aluminium block	480
Structure	Structure	258
SUM		3899.7

The optimal material for insulating sizable areas of containers affixed to the container wall is aerogel. This material exhibits a thermal conductivity in a vacuum of only 0.004 $W.K^{-1}.m^{-1}$. For adequate insulation, a 0.5 mm thick layer is sufficient.

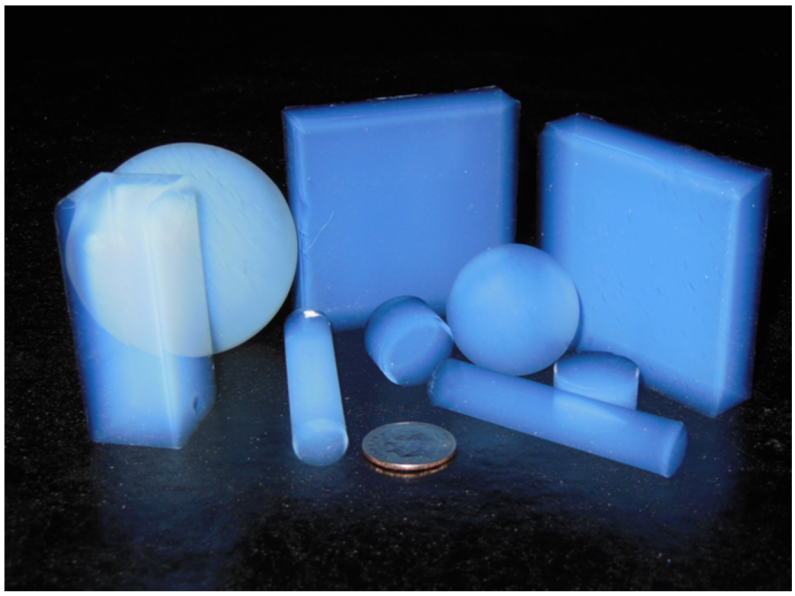

Fig. 1.17: Aerogel

The containers are attached to the packaging with screws. These joints conduct heat well, so they also need to be insulated using aerogel pads as described in chapter **3.1.2.**

Thanks to this approach, it is then necessary to consider only the conductivity of the screw itself. Which can be calculated from its diameter and material, which is stainless steel. The distance through which the heat is transferred is weighted to 4 mm.

Table 7.14: Parameters of M3 screw from stainless steel

Radius r [mm]	**Length L [mm]**	**Conductivity k Cu [W.m^{-1}.K^{-1}]**	**Area A [mm^2]**
1.5	4	16,3	$0.77 \cdot 10^{-6}$

$$C = \frac{kA}{L} = \frac{16{,}3 \cdot 0.77 \cdot 10^{-6}}{4 \cdot 10^{-3}} = 0.027\ W \cdot K^{-1} \tag{7.4}$$

The total value of the thermal conductivity of this contact is 0.5 W/K when using four screws per container and a 0.5 mm thick layer of aerogel. This value was selected based on simulations as a compromise between isolation from external influences and the necessity to cool the containers slightly during the time when the LEDs are running in order to prevent overheating of the bacteria.

7.6.3 Heaters

From the preceding analysis, it can be concluded that the use of heaters is necessary to maintain the cyanobacteria within the requisite temperature range. Termica includes a tool for simulating a thermostat-controlled heater. This model has consistently developed a heater that was switched on frequently, resulting in significant fluctuations in temperature and energy consumption. It is therefore unsuitable for experimental purposes. It is evident that large fluctuations in consumption are detrimental to the electrical system, particularly in the case of batteries. Furthermore, fluctuations in the heating itself, and thus in temperatures, would be lethal to the bacteria. Consequently, a heater with a permanent performance was employed to create a model for both hot and cold cases. During the hot period, the model was created to ensure that there was sufficient heat for the bacteria from the glowing LED. However, these LEDs are programmed to turn off every 12 hours. It is necessary to add heaters with the same power to these windows in order to maintain a stable temperature. In the cold case, it is necessary to turn on the heater to a higher power, since the other subsystems generate only a minimum of heat and the satellite will cool down more. The simulations indicated that each container requires a heater with a power of 2.05 W, resulting in a total required power of 8.2 W. This is a considerable amount of power for a 3U CubeSat. However, this performance is only required when the other subsystems are turned off, which allows for a feasible power budget.

7.7 Final Analysis Results

Once all modifications to the model had been implemented, the results were evaluated in detail in the following chapters.

7.7.1 Cold Case

A review of the values displayed in the accompanying image leads to the conclusion that all subsystems, including the payload, are within their temperature limits. Once more, the batteries are below the temperature limit for charging. However, this deficiency will be resolved by the built-in heater in the battery case.

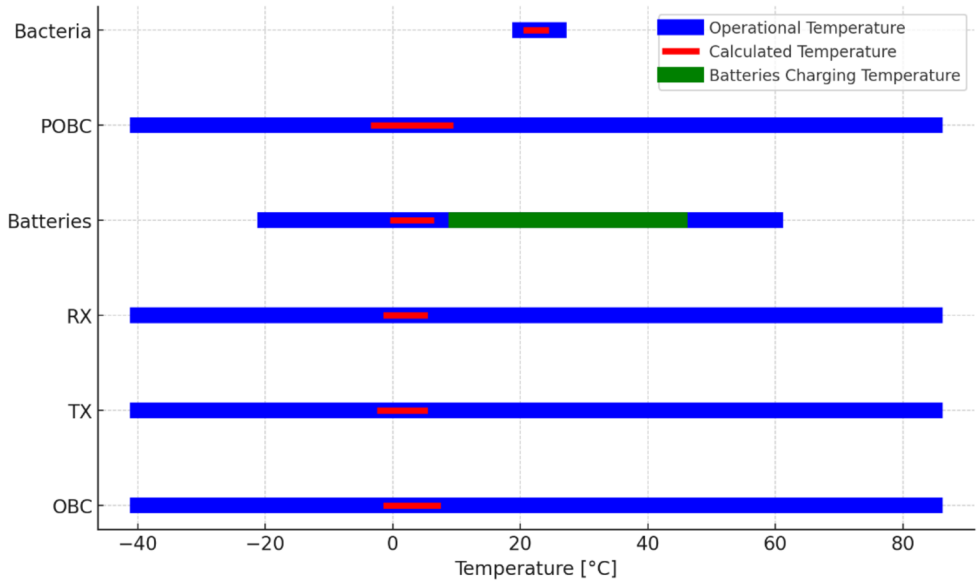

Fig. 7.18: Comparison of operational and calculated temperatures for Cold case

Table 7.15: Temperatures of subsystem for Cold case

	Operational temperatures [C˚]		Calculated temperatures [C˚] (first analysis)		Calculated temperatures [C˚] (final analysis)	
	Min.	Max.	Min.	Max.	Min.	Max.
OBC	-40	85	-11	-5	-1	7
TX	-40	85	-14	-5	-2	5
RX	-40	85	-13	-5	-1	5
Batteries	-20	45	-12	-6	0	6
POBC	-40	85	-16	-10	-3	9
Bacteria	20	26	-21	-4	21	24

A comparison of the values from the initial and final analyses in Table No. 1 reveals that the temperatures of all subsystems have increased. This is a consequence of the heaters added to the payload, which heat the entire CubeSat in this way.

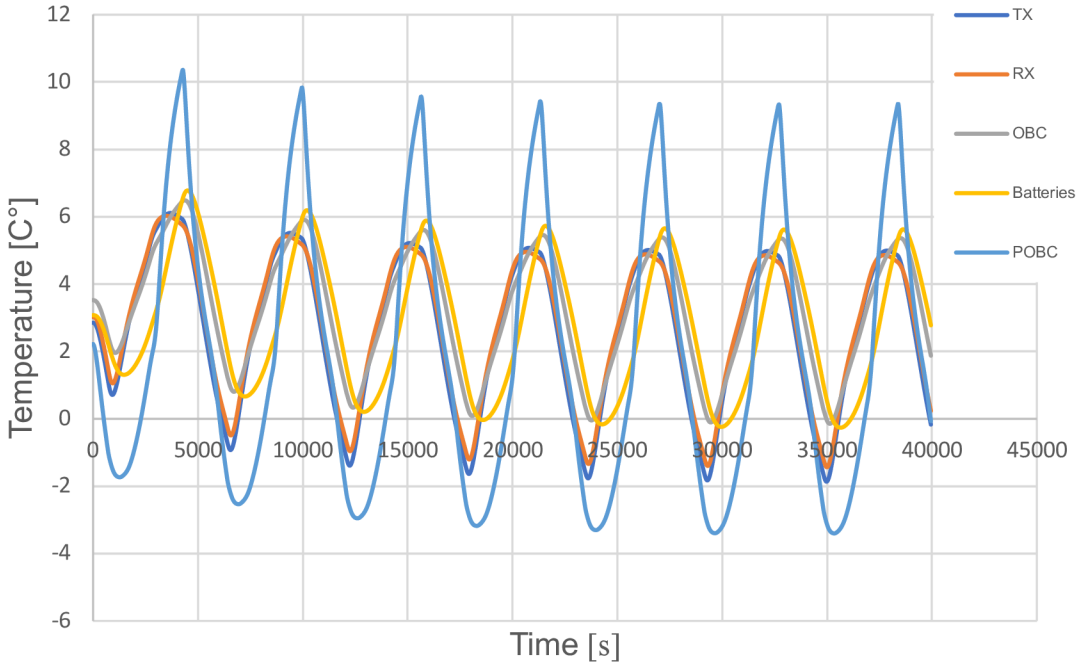

Fig. 7.19: Temperature course of electronic subsystems cold case

Figure 7.19 illustrates a comparison of the development of temperatures on electronic subsystems. The simulation was accurate for 15 orbits; however, due to the clarity of the graph, the last few orbits were omitted. This was because in this case the temperature stabilised rapidly and the development continued in a similar manner. The fast stabilisation is due to the fact that in the cold case the temperature dissipation of the components is minimal and does not change. The graph illustrates that the temperature of the POBC fluctuates the most, which is attributed to the addition of a thermal strip that connects it to the solar panel. This results in a faster cooling and heating rate according to the illumination of the panel. The TX and RX have an essentially identical course, given that they are located on the same PCB.

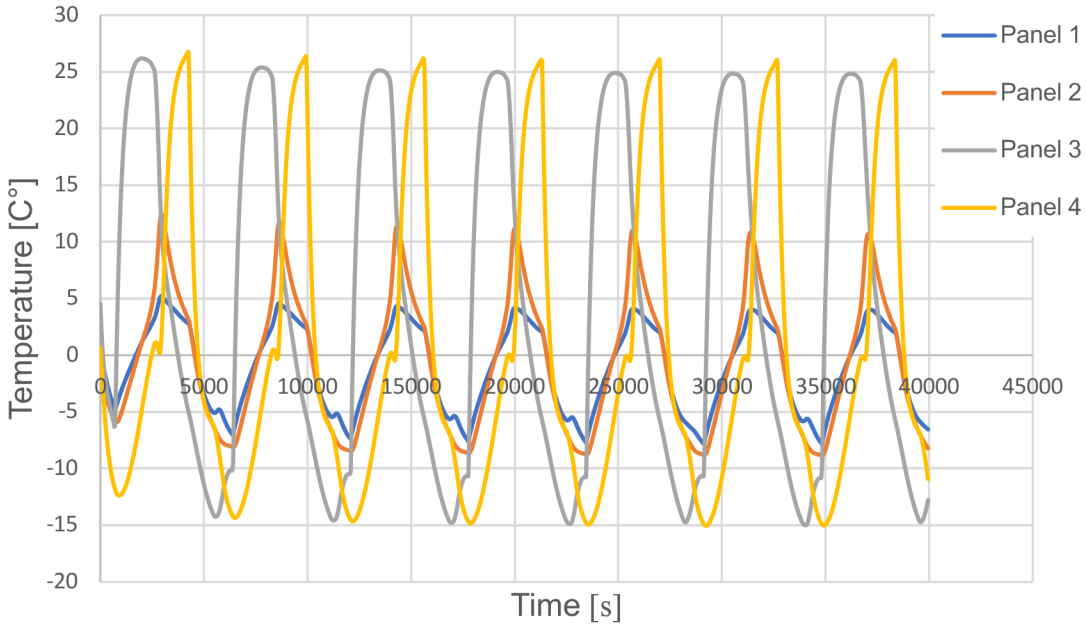

Fig. 7.20: Temperature course of solar panels

The Figure 7.20 depicts the temperature profile of the solar panels during the Hot Case. The regular changes observed on the panels can be attributed to the bound rotation of the satellite, which is equipped with magnets.

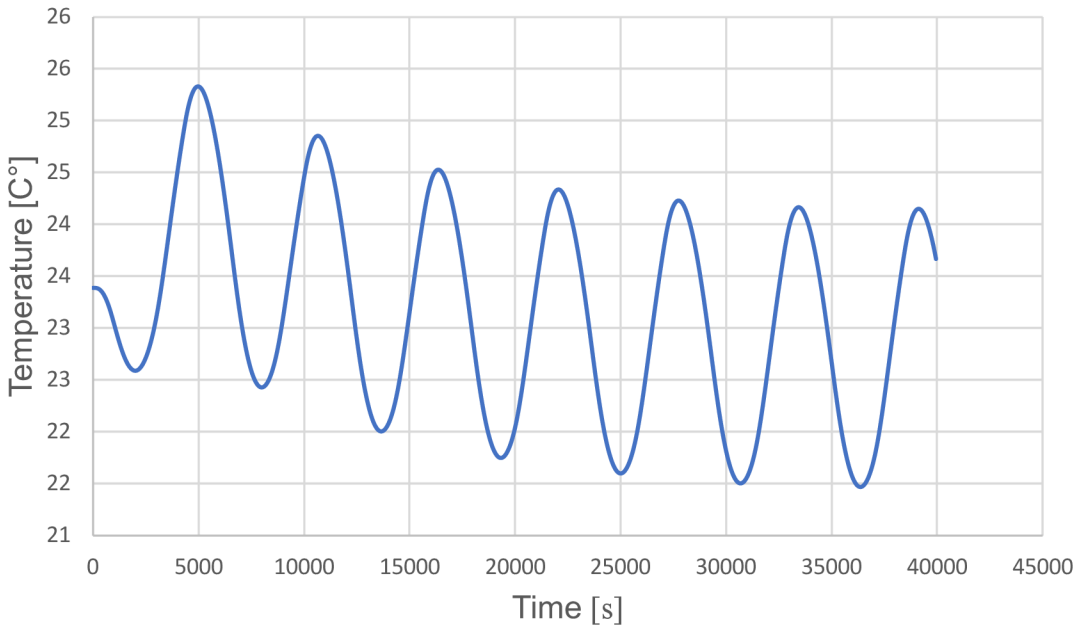

Fig. 7.21: Temperature course of electronic cyanobacteria

Figure 7.21 illustrates the temperature evolution of the bacteria over time. The temperature of the bacteria remains within the recommended range throughout the entirety of the simulation. This is a consequence of the correct balance of insulation, the performance of heaters and the amount of material that holds heat.

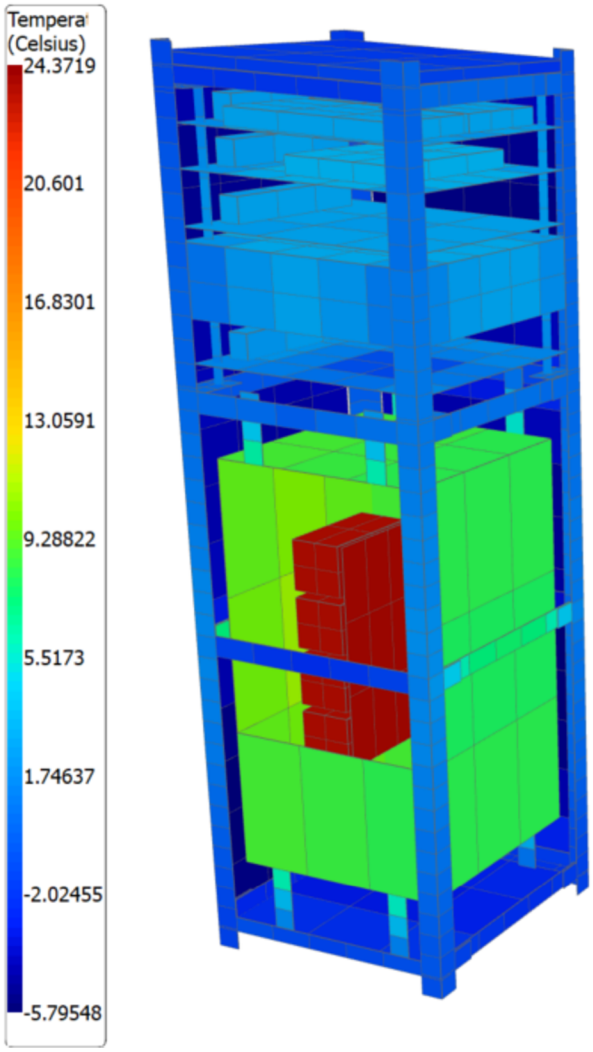

Fig. 7.22: Thermal distribution of the satellite in the shadow

Figure 7.22 illustrates the temperature distribution of the satellite when it is in the shadow of the Earth. A notable temperature differential is evident between the payload, which is subjected to heating, and the remainder of the satellite. The greatest temperature differential is observed between the containers and the MIBICO time, where an airgel with excellent insulating properties is present. On POBC, it is possible to observe a cooler

area. This is the location where the solar panel is connected, which results in a faster loss of heat than in the surrounding components due to this connection.

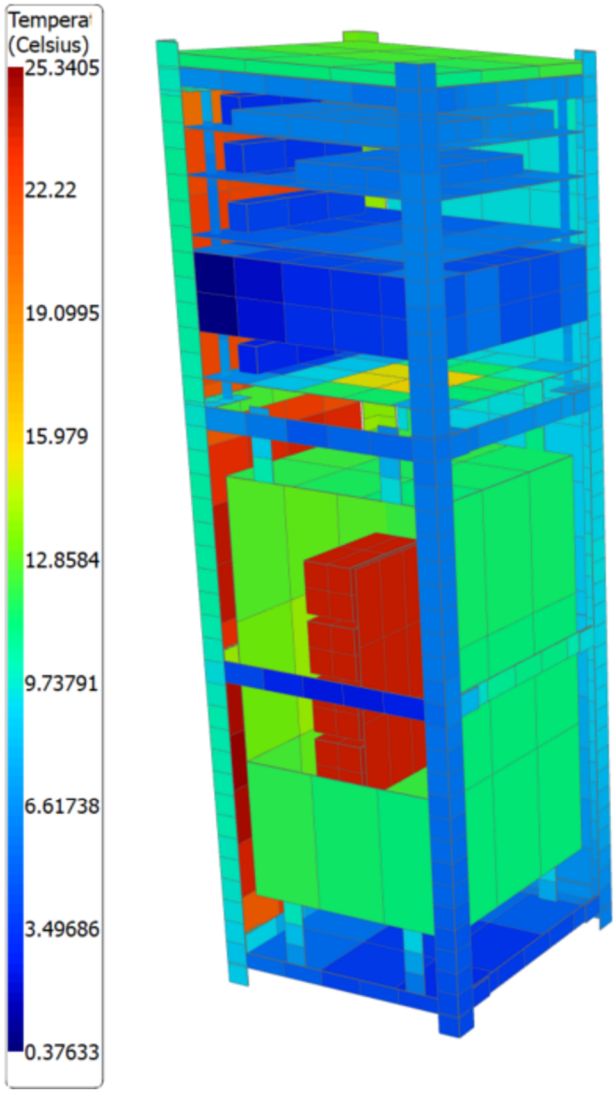

Fig. 7.23: Thermal distribution of the satellite in the sunlight

The Figure 7.23 illustrates the temperature distribution on the satellite when it is in sunlight. It is evident that the POBC is connected to the solar panel, with the glare solar panel in this instance heating the centre of the POBC. The bacteria have a higher temperature due to their surroundings being warmer than in the previous case, thus reducing the rate at which they lose heat to their surroundings.

7.7.2 Hot Case

In the Hot Case, it was also possible to ascertain that all subsystems were within the required temperature limits, as can be seen in the accompanying Figure 7.24

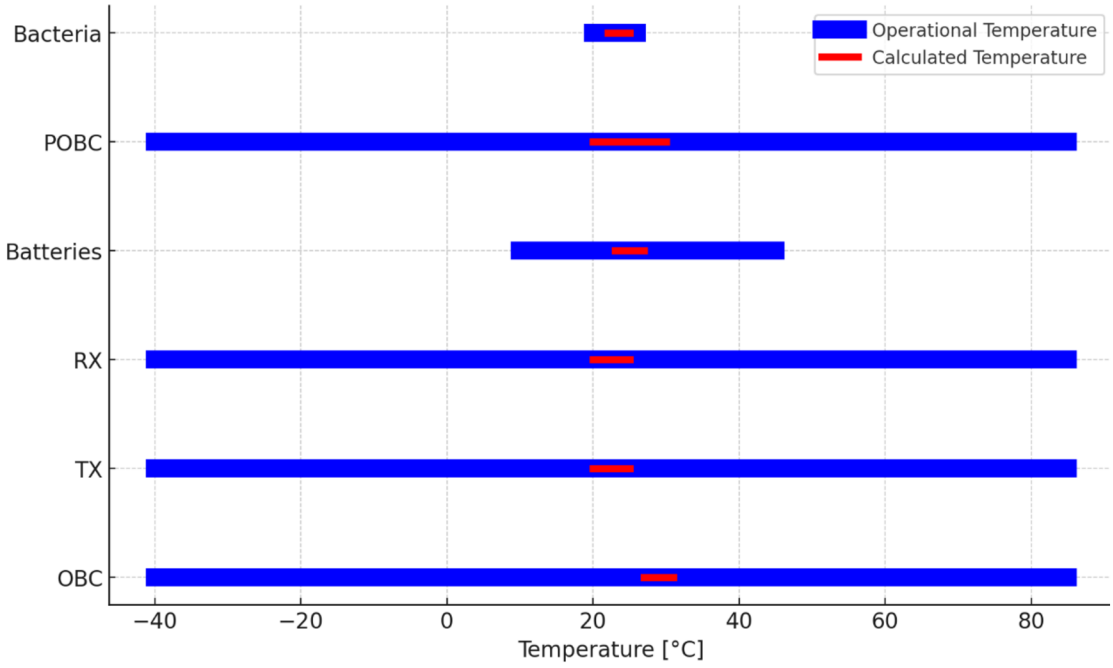

Fig. 7.24: Comparison of operational and calculated temperatures for Hot case

Table 7.16: Temperatures of subsystem for Hot case

	Operational temperatures [C˚]		Calculated temperatures [C˚] (first analysis)		Calculated temperatures [C˚] (final analysis)	
	Min.	Max.	Min.	Max.	Min.	Max.
OBC	-40	85	36	40	27	31
TX	-40	85	28	30	20	25
RX	-40	85	28	30	20	25
Batteries	10	45	35	38	23	27
POBC	-40	85	35	40	20	30
Bacteria	20	26	19	38	22	25

A comparison of the temperatures in the table reveals a decrease in the temperatures of all subsystems. This is attributed to the thermal strip between the POBC and the satellite, which removes heat from the interior of the satellite to the surface, thereby cooling the entire system. It is evident that the temperature fluctuations observed in the

bacteria have been significantly reduced. This outcome can be attributed to the implementation of enhanced insulation and the incorporation of additional material into the payload.

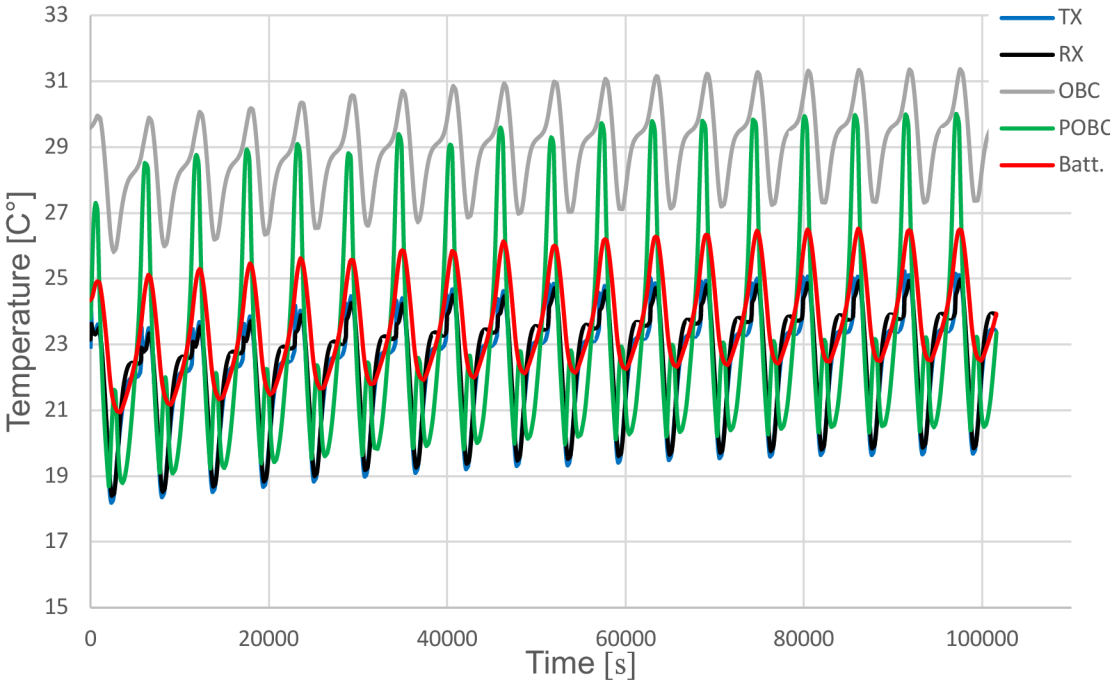

Fig. 7.25: Temperature course of electronic subsystems

The Figure 7.25 depicts the evolution of the temperatures of all electrical subsystems within the Hot Case. In this instance, it was necessary to display a greater number of cycles before the temperatures stabilised. This is due to the greater complexity of the system, as during the hot phase, all devices have greater dissipation, whereas TX dissipates only at certain intervals. From the graph, it can be observed that the OBC has the highest temperature, which is primarily due to its location. This is because it is situated between other subsystems, which limits the options for heat removal. Furthermore, it has high dissipation when it is running at full capacity. Even in Hot Case, the POBC exhibits the greatest temperature fluctuations due to its thermal connection with the solar panel. In contrast, the batteries exhibit the least fluctuations, as they are encased in a PEEK case that effectively isolates them from their surrounding environment. The course of TX and RX is identical, despite the fact that TX has a higher performance. Nevertheless, this performance is not permanent, and they are located on one board, which thermally connects them significantly.

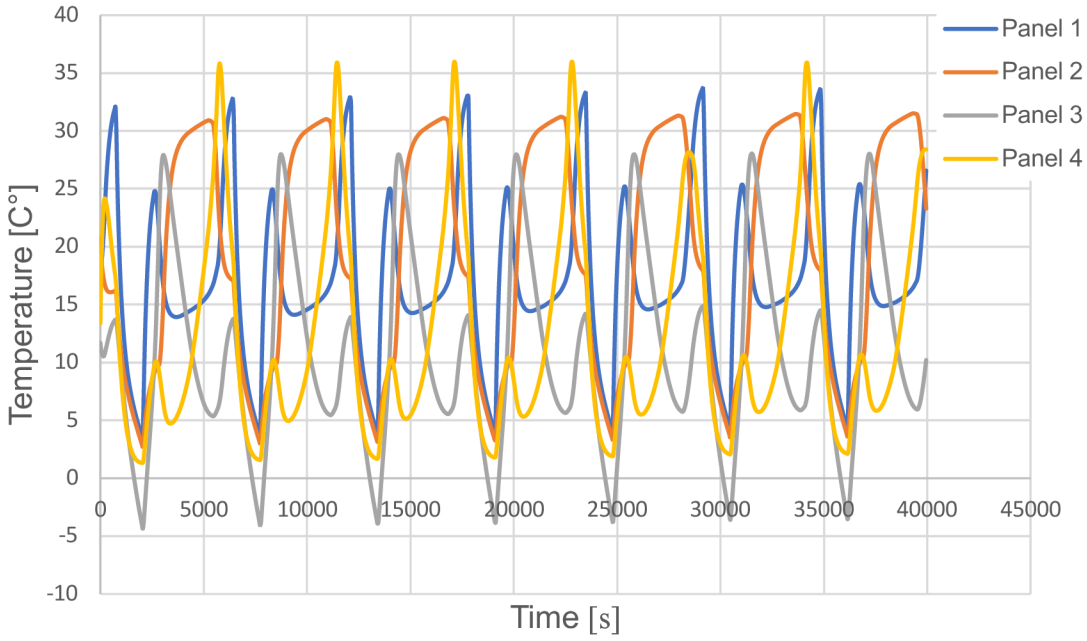

Fig. 7.26: Temperature course of solar panels

The Figure 7.26 depicts the temperature curve of the solar panels. The phenomenon is regular, yet considerably more intricate than the cold case. This phenomenon is the result of the influence of more complex temperature processes on the internal subsystems, which are also manifested on the surface of the satellite.

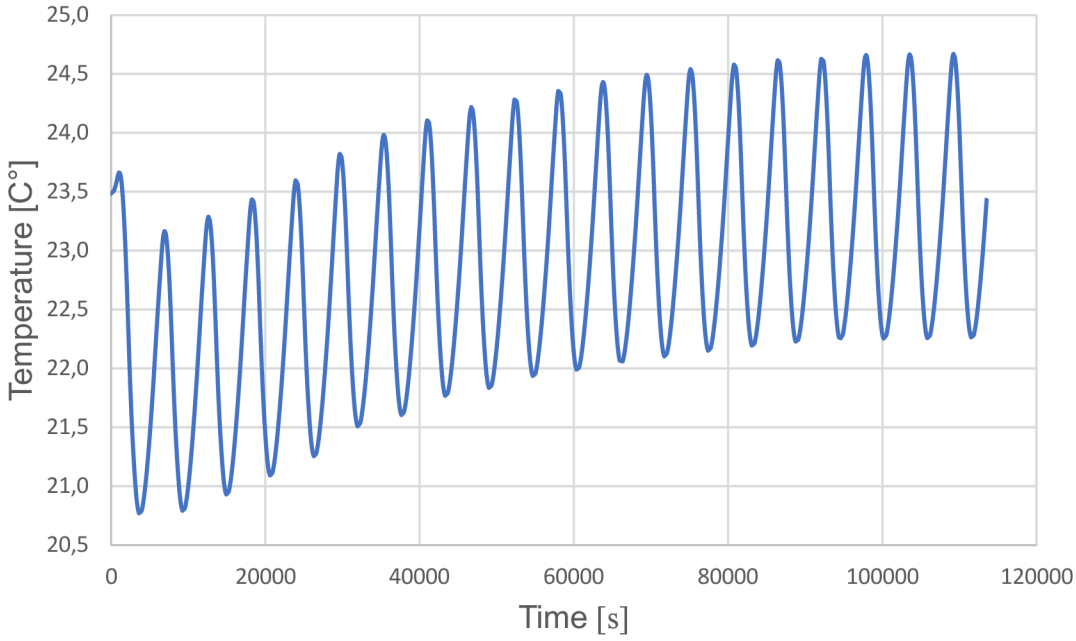

Fig. 7.27: Temperature course of bacteria

The attached Figure 7.27 illustrates the temperature course of the bacteria. It can be observed that in the case of the hot case, it took up to 20 orbits for the temperature to stabilise. Once the temperature has reached a stable equilibrium, it does not fluctuate precisely around 23 degrees, as would be optimal. However, this represents a compromise between the high temperature and the size of the deviations from the centre. The addition of further sealing would result in a reduction in fluctuations, although this would be accompanied by an increase in the average temperature and a reduction in the viability of the bacteria.

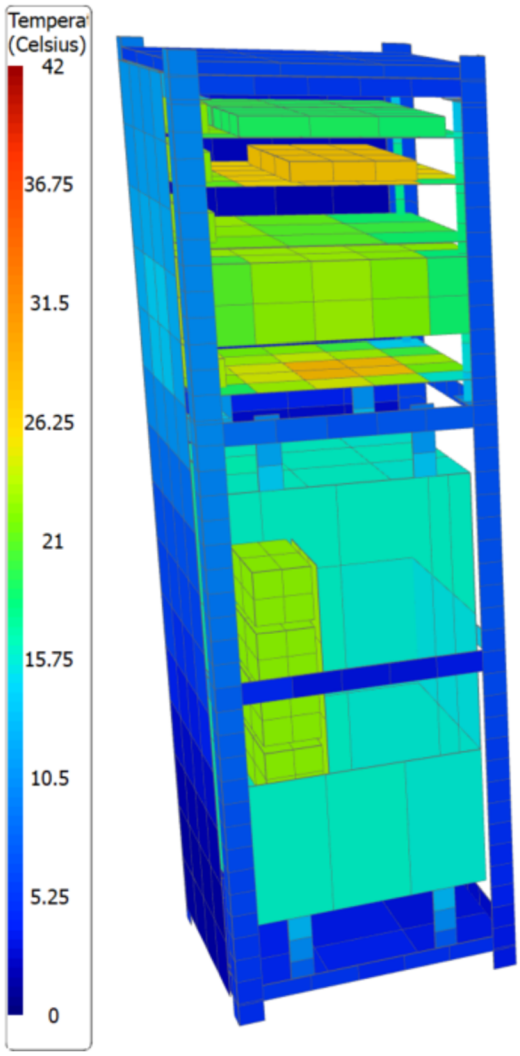

Fig. 7.28: Thermal distribution of the satellite in the shadow

The Figure 7.28 depicts the temperature distribution of the satellite when it is in the shadow of the Earth during the full operation of all subsystems. In the figure, the OBC and POBC are the most conspicuous, exhibiting the highest power and, consequently, the greatest dissipation. Additionally, the warmer region on the left-hand panel is heated by the POBC via a heat strap. The temperature jump is clearly visible in the containers with bacteria, which are isolated from the surroundings.

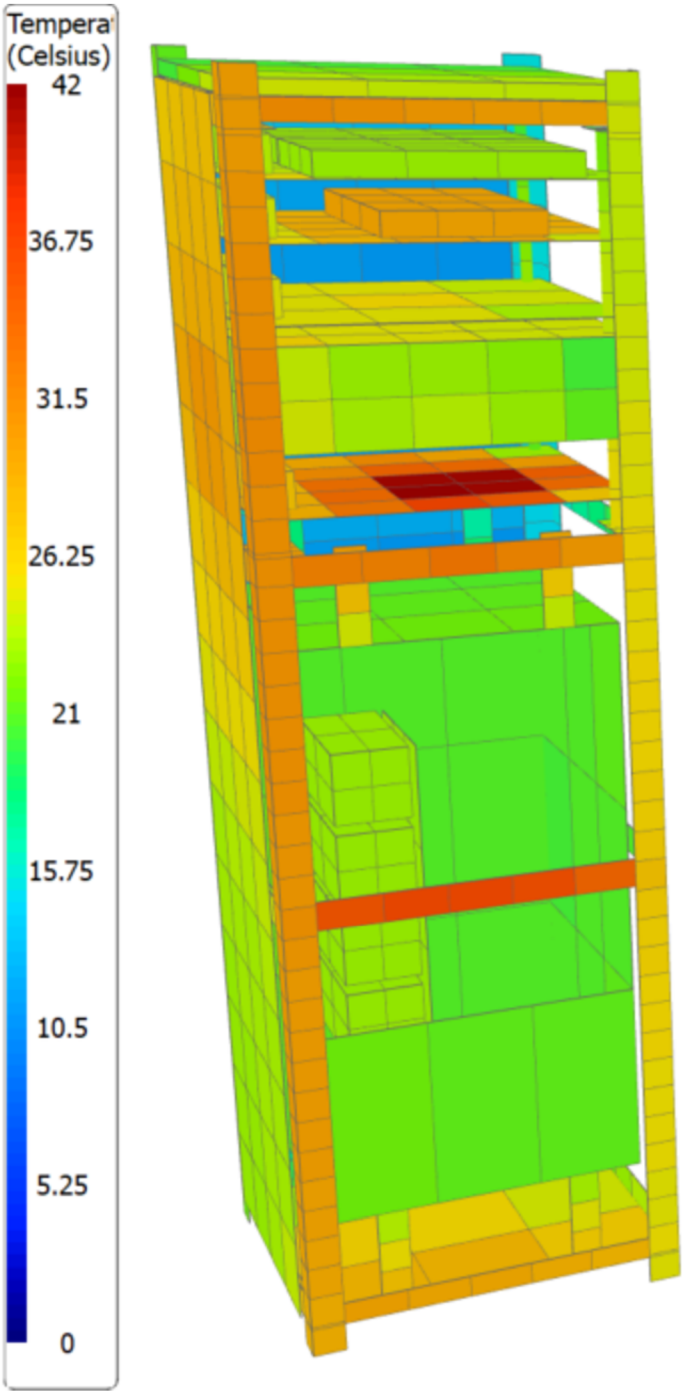

Fig. 7.29: Thermal distribution of the satellite in the shadow

The Figure 7.29 depicts the temperature distribution of the satellite when it is in sunlight during full operation of all subsystems. In this instance, it is evident that the payload case provides effective protection for the bacteria, even in the event of overheating.

CONCLUSION

This work dealt with thermal modelling of satellites in a comprehensive manner. It covered various engineering and scientific areas from the physical background, explanation of space conditions, methods to manage the thermal model, to the mathematical basis of thermal analyses and the programs built upon them.

The description of creating a thermal model demonstrated the complexity of this process, mainly due to the limited exploration of this field and the lack of materials detailing the thermal modelling process and its unique requirements and methods used for nanosatellites. It is very challenging to estimate the thermophysical properties of thermal contacts, which are often complex and rarely can be described in detail numerically, let alone analytically. The most accurate values come from experimental measurements, which are scarce and require special measurements for each material. Another limitation is the technologies themselves, where it is evident that the space industry still focuses primarily on large satellites in terms of thermal control. Many active management technologies have not yet been sufficiently developed and miniaturized for use in nanosatellites.

However, this work shows that it is possible to create a full-fledged and functional thermal model for a nanosatellite. It demonstrates that even with basic passive technologies and heaters, it is possible to design a thermal model that meets the temperature limits necessary for the survival of microorganisms in Earth's orbit. Thus, this work fulfils its primary goal of determining the feasibility of researching the cultivation of cyanobacteria in low Earth orbit.

The successful attainment of this goal was facilitated by the implementation of several thermal management components. Aerogel was utilized to insulate the cyan, a heat strap was employed to dissipate excess heat from the overheated sections of the payload's on-board computer, and heaters were used to warm the cyanobacteria as necessary. These modifications enabled a substantial alteration in the temperature ranges experienced by the cyanobacteria. In the original model, the temperature varied from -21°C to -4°C. However, in the Cold Case analysis, the temperature range was improved to 21°C to 24°C, and in the Hot Case analysis, it was adjusted from an initial range of 19°C to 38°C to a more controlled range of 22°C to 25°C.

The model developed in this work represents a first step in the creation of a functional satellite that can withstand the thermal conditions of space. In the subsequent stages, the thermal behaviour of selected contacts and materials estimated in the model will require experimental verification. The experiment itself will require further definition, after which the findings will need to be incorporated into the future design of the satellite.

In conclusion, this work created a functional CubeSat model and thereby laid the foundation for the next phase of the CIMER project, demonstrating its feasibility from a thermal perspective.

LITERATURE

[1] POGHOSYAN, Armen a GOLKAR, Alessandro. CubeSat evolution: Analyzing CubeSat capabilities for conducting science missions. Online. *Progress in aerospace sciences*. 2017, roč. 88, s. 59-83. ISSN 0376-0421. Available from: https://doi.org/10.1016/j.paerosci.2016.11.002. [cit. 2024-02-25].

[2] NASA. *What are SmallSats and CubeSats?* Online. NASA. 2024. Available from: https://www.nasa.gov/what-are-smallsats-and-cubesats/. [cit. 2024-04-25].

[3] ISISPACE. *ISIPOD CubeSat Deployer*. Online. Available from: https://www.isispace.nl/product/quadpack-cubesat-deployer/. [cit. 2024-05-19].

[4] *Nanosat Database*. Online. 2023. Available from: https://www.nanosats.eu/. [cit. 2024-02-25].

[5] *CubeSat Form Factor Thermal Control Louvers*. Online. NASA Available from: https://technology.nasa.gov/patent/GSC-TOPS-40. [cit. 2024-02-28].

[6] SEDLÁŘ, Martin a MORNSTEIN, Vojtěch. *Zobrazovací metody využívající neionizující záření*. Masarykova univerzita, 2014. ISBN 978-80-210-7156-8.

[7] KREITH, Frank; MANGLIK, R. M. a BOHN, Mark. *Principles of Heat Transfer*. 7th ed. Stamford: Cengage Learning, 2011. ISBN 978-0-495-66770-4.

[8] GILMORE, David (ed.). *Spacecraft Thermal Control Handbook*. 2nd ed. American Institute of Aeronautics and Astronautics, 2002. ISBN ISBN 1-884989-11-X.

[9] *Radiation*. Online. DSPE. 2024 Available from: https://www.dspe.nl/knowledge/thermomechanics/chapter-1-basics/1-2-heat-transfer/radiation/. [cit. 2024-03-20].

[10] PLANTE, Jeannette a LEE, Brandon. *Environmental Conditions for Space Flight Hardware – A Survey*. Dynamic Range Corporation, 2004. Available from: https://view.officeapps.live.com/op/view.aspx?src=https%3A%2F%2Fnepp.nasa.gov%2Fdocuploads%2FC5E0869C-0469-4D11-9FAA8012C8F52351%2Fenvironmental%2520Testing%2520Survey.doc&wdOrigin=BROWSELINK. [cit. 2024-02-29].

[11] MIAO, Jianyin; ZHONG, Qi; ZHAO, Qiwei a ZHAO, Xin. *Spacecraft Thermal Control Technologies*. 1. Springer Singapore, 2021. ISBN 978-981-15-4984-7.

[12] SAWYER, Sam. *Heat Storage and Management with Phase Change Material in CubeSats*. Master thesis. Mekelweg, Netherlands: Delft University of Technology, 2020.

[13] SHI, Qinghai a KANOUN, Olfa. *Automated Wire Fault Location Using Impedance Spectroscopy and Differential Evolution*. 2013.

[14] *Types of orbits*. Online. ESA. 2024. Available from: https://www.esa.int/Enabling_Support/Space_Transportation/Types_of_orbits. [cit. 2024-05-19].

[15] *Solar Influence On The Earth System*. Online. NASA. 2018. Available from: https://sunclimate.gsfc.nasa.gov/article/solar-influence-earth-system. [cit. 2024-03-01].

[16] PRICE, David L a FERNANDEZ-ALONSO, Felix. Experimental Methods in the Physical Sciences. In: *Experimental Methods in the Physical Sciences*. 48. United States: Elsevier B.V, 2015, ii-ii. ISBN 0128020490. ISSN 1079-4042. Available from: https://doi.org/10.1016/B978-0-12-802049-4.21002-6.

[17] KEARNEY, Mike-Alec. *A thermal simulation tool for CubeSats for dynamic in-orbit scenarios, verified with flight data from the nSight-1 mission*. Master thesis. Stellenbosch, South Africa: Faculty of Engineering at Stellenbosch University, 2020.

[18] *Space environment*. Online. ECSS-E-ST-10-04C Rev.1. European Cooperation for Space Standardization, 2020. Available from: https://ecss.nl/standard/ecss-e-st-10-04c-rev-1-space-environment-15-june-2020/. [cit. 2024-03-07].

[19] In: *State-of-the-Art Small Spacecraft Technology*. NASA, 2024, p. 202-221. Available from: https://www.nasa.gov/wp-content/uploads/2024/03/soa-2023.pdf?emrc=8ad1a1. [cit. 2024-04-27].

[20] *CubeSat101*. Online. California Polytechnic State University, 2017. Available from: https://www.nasa.gov/wp-content/uploads/2017/03/nasa_csli_cubesat_101_508.pdf. [cit. 2024-04-25].

[21] ISHIZAWA, Junichiro. *Evaluation of White Paints Exposed to Space Environment on the ISS Russian Service Module / Space Environment Exposure Device*. Online. Ibaraki Japan, 2009. Available from: https://www.jstage.jst.go.jp/article/tstj/7/ists26/7_ists26_Pc_111/_pdf. [cit. 2024-04-27].

[22] *Astrawrap*. Online. Aerospacefab. 2024. Available from: https://aerospacefab.com/products/spacewrap/. [cit. 2024-04-27].

[23] *THERMAL STRAPS*. Online. Technology Applications, Inc. 2024. Available from: https://www.techapps.com/thermal-straps. [cit. 2024-04-27].
[24] *The Basics of Heat Pipes – Their History, Principle, and Varieties explained*. Online. DNP. 2022. Available from: https://www.global.dnp/biz/column/detail/10162360_4117.html. [cit. 2024-04-27].
[25] *Flexible Heater for Space*. Online. SatCatalog. 2024. Available from: https://www.satcatalog.com/component/flexible-heater-for-space/. [cit. 2024-04-28].
[26] *Small Satellite Thermal Modeling Guide*. Online. The Airforce Research Laboratory, 2022. Available from: https://apps.dtic.mil/sti/pdfs/AD1170386.pdf. [cit. 2024-04-28].
[27] WERTZ, James R; EVERETT, David F a PUSCHELL, Jeffery J. *Space mission engineering: the new SMAD*. Torrance: Microcosm Press, 2018. ISBN 978-1-881-883-15-9.
[28] MATURANO, Francisco. *NUMERICAL METHODS FOR COMPUTING THE TEMPERATURE DISTRIBUTION IN SATELLITE SYSTEMS*. Master thesis. Barcelona, Spain: Escola Tècnica Superior d'Enginyeria de Telecomunicació de Barcelona, 2012.
[29] *THERMICA User Guide*. V4.9. AIRBUS DEFENCE AND SPACE, 2022.
[30] MAHAN, J. Robert. *THE MONTE CARLO RAY-TRACE METHODIN RADIATIONHEAT TRANSFERAND APPLIEDOPTICS*. ASME Press and John Wiley, 2018. ISBN 9781119518525.
[31] POVALAČ, Aleš. *Nanosatellite Design and Electronics*. 2021.
[32] *Cubesat Components*. Online. Spacemanic. 2024. Available from: https://www.spacemanic.com/cubesat-components. [cit. 2024-05-11].
[33] *ISISpace*. Online. 2024. Available from: https://www.isispace.nl/. [cit. 2024-05-11].
[34] *MatWeb*. Online. 2024. Available from: https://www.matweb.com/. [cit. 2024-05-14].
[35] *Thermal Analysis and Control of MIST CubeSat*. Master Thesis. STOCKHOLM, SWEDEN: KTH Royal Institute of Technology, 2017.
[36] *PC/104 and PC/104-Plus Application Specification Connectors*. Online PDF. TE connectivity, 2017 Available from: https://www.te.com/commerce/DocumentDelivery/DDEController?Action=showdoc&DocId=Specification+Or+Standard%7F114-

13021%7FC%7Fpdf%7FEnglish%7FENG_SS_114-13021_C.pdf%7F1375795-2. [cit. 2024-05-14].

[37] SHI, Qinghai a KANOUN, Olfa. *Automated Wire Fault Location Using Impedance Spectroscopy and Differential Evolution*. 2013.

[38] *Space Physics: Heat, Temperature, and the Electromagnetic Spectrum*. Online. Cosmicopia. 2013. Available from: https://cosmicopia.gsfc.nasa.gov/qa_sp_ht.html. [cit. 2024-05-15].

[39] *Natural Rubber*. Online. MatWeb. 2024. Available from: https://www.matweb.com/search/DataSheet.aspx?MatGUID=da912e0c50154649a201d8f7abbf7e90&ckck=1. [cit. 2024-05-19].

[40] *Aluminum 6061-T6*. Online. MatWeb. 2024. Available from: https://www.matweb.com/search/DataSheet.aspx?MatGUID=b8d536e0b9b54bd7b69e4124d8f1d20a. [cit. 2024-05-19].

[41] HONG, Yu. *Thermal parameters of cylindrical power batteries: Quasi-steady state heat guarding measurement and thermal management strategies*. Shanghai University of Engineering Science. Available from: https://web.me.iastate.edu/wang/2023%20Applied%20Thermal%20Engineering.pdf.

[42] *MatWeb*. Online. Copper, Cu; Annealed. 2024. Available from: https://www.matweb.com/search/DataSheet.aspx?MatGUID=9aebe83845c04c1db5126fada6f76f7e. [cit. 2024-05-19].

[43] *MatWeb*. Online. Röhm Acrylite® GP Acrylic Sheet, Cast. 2024. Available from: https://www.matweb.com/search/DataSheet.aspx?MatGUID=a3b8b49ec66b4896bbade55dbd271ddd. [cit. 2024-05-19].

SYMBOLS AND ABBREVIATIONS

Abbreviations:

P-POD	A Poly Picosatellite Orbital Deployer
LEO	Low Earth Orbit
MEO	Medium Earth Orbit
GEO	Geostationary Orbit
TCS	Thermal Control System
ISS	International Space Station
MLI	Multi-Layer Insulation
PCM	Phase Change Materials
FEM	Finite Element Method
FDM	Finite Difference Method
RCN	Reduced Conductive Network
CIMER	Cyanobacteria In Microgravity Environment Research\
OBC	On-Board Computer
POBC	Payload On-Board Computer
EPS	Electrical Power System
COMs	Communication system
PCB	Printed Circuit Board

Symbols:

q_k	conduction	$(W.K^{-1})$
k	conductivity	$(W.m^{-1}.K^{-1})$
A	area	(m^2)
T	thermodynamic temperature	(K)
E	energy	*(eV)*
h	Planck constant	$(kg.m^2.\ s^{-1})$
f	frequency	(Hz)
c	speed of light	$(m.s^{-1})$
λ	wavelength	(m)
b	Wien's constant	(m.K)
q_r	heat flow rate	(W)
σ	Stefan-Boltzman constat	$(W.m^{-2}.K^{-4})$
P	total power of Sun	(W)
ε	emissivity	(-)
a	absorptivity	(-)
F	view factor	(-)